Structures 91 (2026) 112715

Contents lists available at ScienceDirect

Structures

journal homepage: www.elsevier.com/locate/structures

Advanced non-linear quasi-static and dynamic analysis of historical masonry buildings accounting for the spatial anisotropy of the structural response

Luigi Salvatore Rainone [a], Elisa Bertolesi [b,*], Giuseppina Uva [a], Siro Casolo [c]

[a] DICATECh Department, Politecnico di Bari, Bari, Italy
[b] Cardiff School of Engineering, Cardiff University, Cardiff, United Kingdom
[c] ABC Department, Politecnico di Milano, Milano, Italy

ARTICLE INFO

Keywords:
Masonry aggregate
Buildings anisotropy
Seismic directionality
Pushover
Non-Linear Dynamic Analyses

ABSTRACT

The proposed study aims to investigate the Non-linear Quasi-Static and dynamic response of historic masonry buildings explicitly accounting for the planimetric anisotropy of the structural response. Historic masonry buildings frequently exhibit irregular geometry and a heterogeneous spatial distribution of material mechanical properties. As a result, the structure exhibits different responses depending on the direction in the horizontal plane along which the applied horizontal action acts, whether under static or dynamic loading. To investigate how this anisotropy influences the evaluation of structural safety, the present study uses Non-Linear Quasi-Static and Dynamic Numerical Analyses by rotating the reference system for the application of the loading. In this work Palazzo Carmelo, a historic building located in the city of Cerignola (Apulia, Southern Italy), is adopted as a case study. The building is characterised by a highly irregular plan layout and a heterogeneous distribution of structural element strength, making it a comprehensive and complex case study with data available in the literature. A detailed 3D Finite Element model of this case study is developed in ABAQUS. The mechanical behaviour of the materials is modelled through the available Concrete Damage Plasticity constitutive law. The results highlight that, within the numerical modelling of historic masonry buildings, evaluating the anisotropy of the structural response is of significant importance and should be systematically incorporated into engineering practice.

1. Introduction

The numerical modelling and structural safety assessment of existing buildings are affected by numerous sources of uncertainty [1–5]. As noted by Rota et al. [4], these sources of uncertainty are associated with the process of knowledge acquisition and mechanical parameter identification, the assumptions underlying the numerical model, the definition of displacement and strain thresholds for the relevant limit states, and the characterization of the seismic input.

The geometric characterization of masonry buildings is a complex task due to their frequent location within building aggregates (Fig. 1), where shared walls, structural interactions with adjacent units, hidden discontinuities and limited accessibility often prevent a complete description of the actual structural configuration. Similarly, mechanical characterization is affected by the intrinsic variability of the materials employed, the heterogeneity of masonry textures, and the difficulty of performing extensive in-situ experimental investigations, which are essential for the global characterization of a given masonry typology [6]. In this context, non-destructive testing (NDT), despite being able to support the knowledge process, generally provides local information and their results must be critically interpreted when transferred to the scale of the whole structural model [7]. Furthermore, the presence of pre-existing damage patterns introduces additional uncertainty in both structural characterization and modelling, suggesting, in research contexts, the development of advanced computer-vision approaches for damage detection and mapping [8], which, at present, are still largely not applicable in ordinary professional practice.

In addition, the numerical modelling of masonry assemblages

* Corresponding author.
E-mail addresses: l.rainone@phd.poliba.it (L.S. Rainone), bertolesie@cardiff.ac.uk (E. Bertolesi), giuseppina.uva@poliba.it (G. Uva), siro.casolo@polimi.it (S. Casolo).

https://doi.org/10.1016/j.istruc.2026.112715
Received 17 February 2026; Received in revised form 21 July 2026; Accepted 23 July 2026
Available online 29 July 2026

remains an open challenge in scientific research [9–11], often requiring the adoption of constitutive models based on mechanical parameters that are difficult to measure and therefore highly uncertain. The reliability of seismic assessment procedures is consequently strongly influenced by modelling choices, including the representation of masonry mechanical behavior, diaphragm action, connections between structural components, boundary conditions and interaction with adjacent buildings. This issue is particularly relevant for irregular unreinforced masonry buildings, for which previous studies have shown that different modelling strategies may lead to non-negligible differences in the predicted non-linear response and capacity assessment (Aşıkoğlu et al., 2020).

Existing masonry constructions were generally not designed to resist horizontal actions; therefore, the spatial variability of seismic loading represents a dominant source of uncertainty [4] that must be carefully modelled. This spatial variability arises both from the propagation of the seismic wave itself [12] and from its angle of incidence relative to the structure under investigation [13] (Fig. 2). The latter aspect, together with the geometric configuration of the building and the spatial distribution of the strength of structural elements and must be explicitly considered in safety assessments. Consequently, the anisotropy of the structural response represents a relevant factor in the safety evaluation of masonry buildings, as it can significantly affect the determination of the safety factor against horizontal actions.

Within this context, the present work investigates the effects of the interrelation between the spatial anisotropy of the structure and the directionality of the earthquake on the evaluation of Engineering Demand Parameters (EDPs) for existing masonry buildings. Palazzo Carmelo, a historic building located in Cerignola (Apulia, Italy) for which data are available in the literature [14], is selected as a case study. Its structural behaviour is analysed through 32 Non-Linear Quasi-Static Analyses and 96 Non-Linear Dynamic Analyses, by varying the direction of load application and considering different control points and different EDPs. An advanced and detailed Finite Element model of the case study is implemented in ABAQUS [15], adopting the Concrete Damage Plasticity constitutive model [16,17] to simulate the post-elastic behaviour of the materials identified through in-situ investigations.

The manuscript is organised as follows. Section 2 addresses the problem of modelling the spatial variability of seismic action. Section 3 presents the methodology adopted. Section 4 provides a detailed description of the selected case study, while Section 5 illustrates the implemented numerical model. Sections 6, 7, and 8 present the results obtained from modal analysis, pushover analysis, and Non-Linear Dynamic Analysis, respectively. Section 9 compares the outcomes of the Non-Linear Static and Non-Linear Dynamic Analyses. Finally, Section 10 reports the concluding remarks and outlines future developments of the work.

2. Spatial variability of seismic motion and structural response anisotropy in complex masonry aggregates: state of the art and open issues

The spatial variability of seismic action arises from the spatial variation of seismic wave characteristics during propagation and from the spatial variability of the angle of incidence relative to the structure. The first type of spatial variability is governed by wave dispersion and differential superposition, the *wave-passage effect*, a wave attenuation due to geometric spreading and energy dissipation, and site effects (topographic and geological), which influence the local seismic response [12,18,19]. In particular, [19] demonstrated that this form of spatial variability has a significant influence on the structural response of buildings. The second type of spatial variability also plays a key role in defining the structural response of existing buildings which, due to their highly irregular geometries, may develop collapse mechanisms that depend on the angle of incidence of the seismic action [13]. In this regard, [13] provide a review of more than 80 studies on this topic, highlighting that, over time, researchers have addressed this issue using different analysis strategies, namely *Response Spectrum Analysis* (RSA), *Linear Response History Analysis* (LRHA), *Non-Linear Static Analysis* (NSA), and *Non-Linear Response History Analysis* (NRHA). This issue is also relevant in professional practice, as Italian building code requires the structural response to be evaluated under seismic actions applied along different horizontal directions [20,21].

Research on this topic has predominantly addressed reinforced concrete and steel buildings [22–26]. With specific reference to masonry structures, [27] investigated the behaviour of the Gualtieri Building in L'Aquila by means of Non-Linear Quasi-Static Analyses performed for different loading directions, highlighting the existence of critical directions associated with reduced structural capacity and ductility. Kesavan & Menon [28] proposed a Non-Linear Static approach for masonry buildings based on the N2 method in order to account for the effect of the angle of incidence of the seismic action. Kalkbrenner et al., [29] carried out a series of pushover analyses on the three-dimensional model of Palacio Pereira in Santiago de Chile, rotating the loading direction from 0° to 360°, and observed that the adopted methodology enables a more accurate assessment of structural vulnerability by capturing different collapse mechanisms.

Drawing on the existing literature, this work analyses the anisotropic structural response of a complex historic masonry aggregate with a highly irregular plan configuration and a strongly heterogeneous distribution of structural element strength. Furthermore, the variability of Engineering Demand Parameters (EDPs) related to the adopted control point, which plays a key role in the safety assessment of existing buildings [30,31], is explicitly considered.

Fig. 1. – Example of the irregular configuration commonly observed in masonry structural aggregates (images from Biccari, a historic town in Southern Italy).

Fig. 2. Urban morphology surrounding the case-study building (highlighted in blue), characterised by an irregular arrangement of adjacent buildings. Adapted from: https://pugliacon.regione.puglia.it/web/sit-puglia-sit/finalita-e-contenuti#mains).

3. Methodology for evaluating the impact of aggregate anisotropy on the seismic response

In order to study the effects induced by the spatial variability of seismic action, Non-Linear Quasi-Static and Non-Linear Dynamic Analyses are carried out by varying the angle of incidence of the applied load. The reference system adopted to describe the spatial configuration of the structure is an orthonormal Cartesian coordinate system $\{o,x,y,z\}$, with the structure extending in plan within the $\{x,y\}$ plane and in height along the $\{z\}$-axis. The $\{x\}$-axis is aligned with the West–East cartographic direction, whereas the $\{y\}$-axis is aligned with the South–North cartographic direction.

A generic direction in the $\{x,y\}$ plane, denoted as $\{p\}$, is defined by the counterclockwise rotation angle θ measured from the x-axis. For Non-Linear Quasi-Static Analyses, this direction is adopted as the pushover direction (Fig. 3a). The structural response is assessed for varying values of θ in terms of force, displacement, and stiffness components along the x, y e p axes. For Non-Linear Dynamic Analyses, three sets of accelerograms are considered, each consisting of three components: WE, SN, and UP. These components are applied in the reference system $\{O,\ \xi,\ \eta, z\}$, such that the WE component of the seismic input is aligned along the ξ-axis, the SN component along the η-axis, and the UP component along the z-axis (Fig. 3b). The auxiliary reference system $\{O,\ \xi,\ \eta, z\}$ is defined by the counterclockwise rotation angle θ of the ξ-axis with respect to the x-axis. Accordingly, for $\theta = 0°$, the two reference systems coincide, and the set of accelerograms is applied along the actual geographic directions. In the case of Non-Linear Dynamic Analyses, the structural response is evaluated in terms of forces, displacements, and accelerations in the $\{O,\ \xi,\ \eta, z\}$ reference system.

4. Case study: Palazzo Carmelo in Cerignola (Italy)

Palazzo Carmelo is a historic building dating to the late seventeenth century, located in the historic centre of Cerignola (Apulia, Italy). It was originally constructed as a convent for the Carmelite Friars and subsequently served as the Municipal Administration headquarters from the late nineteenth century until the 1990s, when it was abandoned and the municipal offices were relocated to a new building. The complex is part of a masonry building aggregate (Fig. 4a), has a total covered area exceeding 1000 m^2, and consists of two storeys. Its layout is characterised by a central courtyard with a double staircase connecting the two levels and by a rear garden (Fig. 4b).

The investigated building has a strongly irregular plan, with maximum overall dimensions of about 70 m in the longitudinal direction and 48 m in the transverse direction. The structure develops over 2 levels above ground, with an overall height of approximately 13 m. The

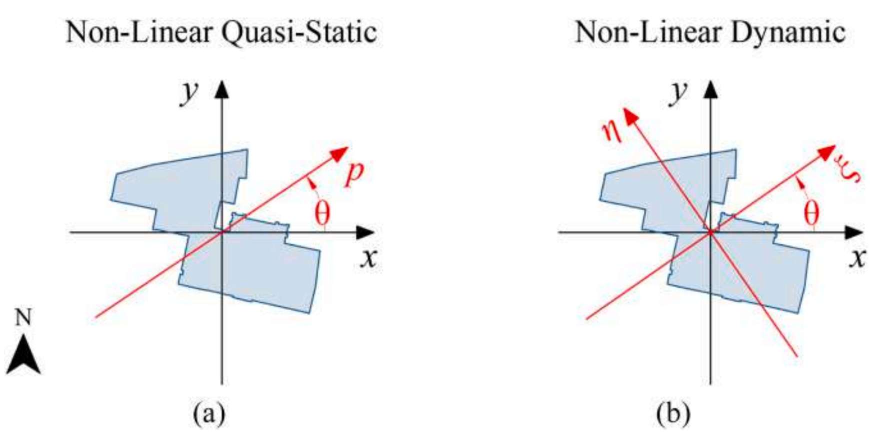

Fig. 3. Schematic representation of the variation in the loading direction and in the reference system of the seismic action for Non-Linear Quasi-Static (a) and Non-Linear Dynamic (b) Analyses.

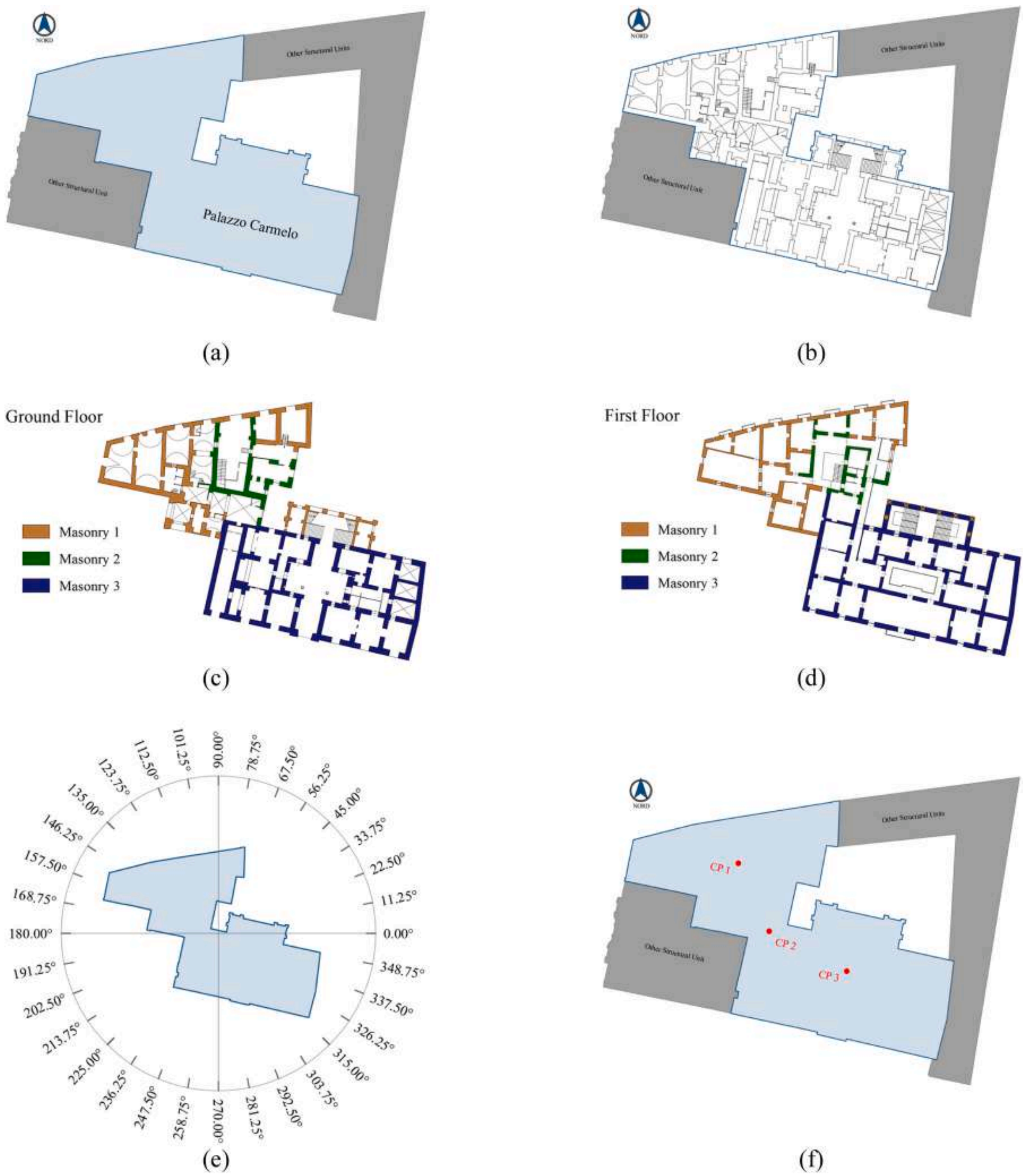

Fig. 4. Palazzo Carmelo: (a) location of the case study within the masonry building aggregate; (b) ground-floor plan; (c–d) spatial distribution of the identified masonry typologies; (e) directions considered for the analysis of the spatial variability of seismic action; (f) control points adopted in the analyses.

vertical load-bearing system consists mainly of masonry walls, whose thickness varies depending on the location and elevation. In particular, the main perimeter walls have thicknesses ranging from approximately 0.75 m to 1.00 m, while the internal masonry walls are generally characterized by thicknesses between 0.60 m and 0.80 m. The floors identified in the building are characterized by different construction typologies, including steel beam floors with hollow clay elements or clay tiles, reinforced concrete joist floors with hollow clay blocks/tiles, and local vaulted masonry systems above suspended ceilings. In several inspected areas, the horizontal structures also include concrete topping or screed layers.

The structural geometry and material properties were defined through an experimental investigation program including thermographic surveys, direct masonry and floor inspections, video-endoscopic examinations, flat-jack tests, magnetometric measurements on reinforced concrete elements, Leeb hardness tests on metallic components, penetrometric tests on mortar, and laboratory characterisation of mortar and plaster samples. The investigation program led to the identification of three main masonry typologies. The first typology consists of quasi-periodic calcarenite masonry, made of squared calcarenite blocks arranged in regular horizontal courses with staggered vertical joints. The second typology corresponds to quasi-periodic coursed calcarenite masonry, also made of squared calcarenite blocks arranged in regular horizontal courses, but characterized by the presence of brick levelling courses consisting of solid clay bricks placed on edge and arranged in three horizontal courses. The third typology is irregular rubble masonry, composed of disordered stone material, including calcarenite and other stones, with blocks of different sizes and an irregular arrangement. Their distribution within the building is shown in Figs. 4c and 4d. For clarity, a specific label is assigned to each masonry typology. The corresponding mechanical properties, derived according to the Italian building code, are reported in Table 1.

5. Advanced FE numerical modelling of the case study

This section outlines the geometric and mechanical characteristics of the implemented model. In particular, Section 5.1 provides a detailed description of the model geometry and of the element types employed, while Section 5.2 presents the adopted constitutive model and the mechanical properties assigned to the structural elements.

5.1. Geometrical modelling

The numerical modelling of the building under investigation is carried out using the Finite Element software ABAQUS [15]. A detailed 3D Finite Element model is developed within the reference system $\{o, x, y, z\}$ defined in Section 3. Since detailed information on the actual quality of wall-to-wall and floor-to-wall connections is not available for the whole structure, these connections are not explicitly modelled. Accordingly, intersecting masonry walls and floors are assumed to be continuously connected. Therefore, the model is constructed by assembling shell elements positioned along the centroidal axes of the surveyed structural components, and the thickness of each shell element is assigned according to the corresponding structural element. This modelling assumption is considered suitable to obtain a good estimation of the structural behavior in Quasi-Static and Dynamic load conditions.

This modelling strategy ensures an accurate representation of the inertial and strength characteristics of the real structural components. The numerical model employs a mixed mesh composed of 47,921 linear quadrilateral elements of type S4 and 894 linear triangular elements of type S3, resulting in a total of 48,815 elements and 50,071 nodes. The S4 element is a four-node, general-purpose, fully integrated, finite-membrane-strain quadrilateral shell element, whereas the S3 element is a three-node general-purpose triangular shell element with finite membrane strains. The adopted mesh is shown in Fig. 5. Fixed boundary conditions are applied at the base of the model to simulate the restraint provided by the foundation system. It is worth mentioning that the current study neglects the interaction with adjacent buildings to avoid introducing additional sources of uncertainty into the modelling process.

5.2. Mechanical modelling

The modelling of the mechanical behaviour of the material is discussed in Section 5.2.1 for the elastic regime and in Section 5.2.2 for the post-elastic regime.

Table 1
Mechanical properties of the materials, with $\sigma_{c,y}$ uniaxial compressive strength, $\sigma_{t,y}$ uniaxial tensile strength, E Young's modulus.

Structural material	Label	Density [kg/m³]	$\sigma_{c,y}$ [MPa]	$\sigma_{t,y}$ [MPa]	E [MPa]
Calcarenite Masonry	Masonry 1	2141	1.949	0.292	1200.00
Coursed Calcarenite Masonry	Masonry 2	2243	2.338	0.351	1200.00
Irregular Rubble Masonry	Masonry 3	1632	0.981	0.147	1000.00

5.3. Linear elastic constitutive model

To model the post-elastic behaviour of the material using the Concrete Damage Plasticity (CDP) model (described in the following section), an isotropic elastic behaviour must be assumed. For each masonry typology, the elastic modulus reported in Table 1 is adopted, while a representative literature value of Poisson's ratio equal to 0.15 is assumed [10,32]. With regard to the floor system, a sufficiently high in-plane stiffness ($E = 2.5E^{10}$ Pa, $\nu = 0.15$) is assigned to the floors to enforce an approximately rigid diaphragm behaviour relative to the masonry walls, consistently with the code-recommended rigid diaphragm assumption.

5.4. Post-elastic hysteretic behaviour

The post-elastic behaviour of the materials is modelled by adopting the Concrete Damage Plasticity Material Model (hereafter CDP). This constitutive model was originally developed to describe damage and cracking processes in concrete-like materials [16,17]. Owing to its availability in the ABAQUS material library, the CDP model is also widely adopted for the numerical simulation of masonry structures, enabling efficient analyses at both sub-assembly and building scales [10,33–41]. The CDP formulation requires the definition of a set of parameters governing the yield surface, the flow-rule, and the visco-plastic regularization. For a detailed description of these aspects, the reader is referred to the ABAQUS documentation [15]. In the absence of specific experimental data for the investigated materials, the following parameter values are assumed: $\psi = 15^\circ$ for the dilatancy angle; $\epsilon = 0.1$ for the eccentricity of the potential flow rule; $\sigma_{b0}/\sigma_{c0} = 1.16$ for the ratio between the equi-biaxial compressive initial yielding stress and the uniaxial compressive initial yielding stress; $K_c = 2/3$ for the parameter that modifies the Drucker-Prager yield function [42]; $\mu = 0.005$ for the viscosity parameter associated with the generalized Duvaut–Lions visco-plastic regularisation scheme [43].

It should be noted that the tensile softening branch of the CDP model was defined in terms of cracking strain. This modelling choice is consistent with the adopted numerical framework and with the level of material information available for the case study. However, it is acknowledged that strain-based softening formulations may lead to mesh-dependent results when tensile damage localizes in quasi-brittle materials. In the present work, this limitation is partly mitigated by the comparative nature of the study, since the same mesh discretization, material parameters, boundary conditions and analysis settings were adopted for all seismic incidence angles. Therefore, the damage patterns are mainly interpreted in qualitative and comparative terms, while the discussion is primarily based on global response indicators.

The post-elastic behaviour of masonry is described through a multilinear skeleton curve, defined according to the laws commonly used for quasi-brittle materials and masonry, consisting of an initial elastic branch followed by strength degradation in the post-peak range [44]. A qualitative representation of the skeleton curve is provided in Fig. 6. For illustrative purposes, a simplified hysteretic response is also shown in the same figure (red line) to illustrate the cyclic behaviour implied by the constitutive model. The points defining the compressive branch (Table 2) of the skeleton curve are expressed in terms of compressive stress σ_c and inelastic strain $\tilde{\varepsilon}_c^{in}$, whereas those defining the tensile branch (Table 3) are expressed in terms of tensile stress σ_t and cracking strain $\tilde{\varepsilon}_t^{ck}$.

Within the CDP framework, material degradation is governed by a scalar damage variable d, which reduces the elastic modulus according to Eq. 2, where E_0 is the initial (undamaged) Young's modulus of the material.

$$E_{damaged} = (1 - d)E_0 \tag{2}$$

The scalar damage variable d depends on the stress-state variables s_t

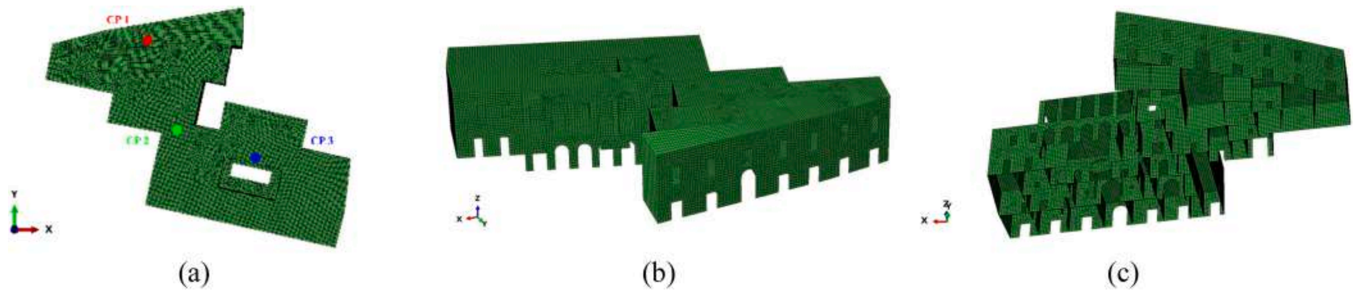

Fig. 5. Numerical model developed in ABAQUS: (a) plan view with control points; (b) upper axonometric view; (c) lower axonometric view.

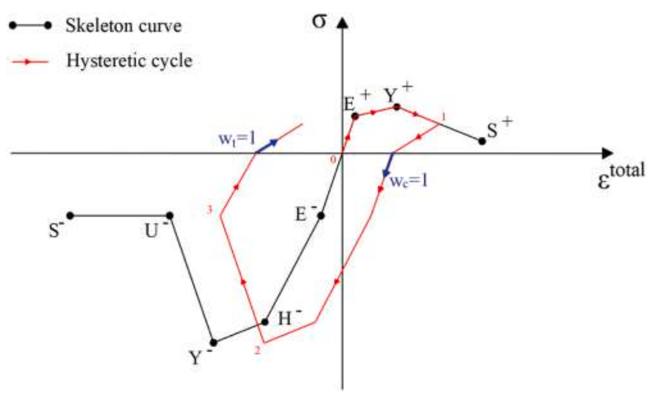

Fig. 6. Multilinear hysteretic stress–strain law adopted to describe the post-elastic behaviour of masonry.

Table 2 –
CDP parameters in compression adopted for the masonry materials.

Material	Point	Inelastic Strain $\tilde{\varepsilon}_c^{in}$ [‰]	Uniaxial Compressive Stress σ_c [MPa]	Damage in Compression d_c [-]
Masonry 1	E^-	0.000	0.643	0.00
	H^-	1.556	1.559	0.00
	Y^-	3.311	1.949	0.00
	U^-	4.669	0.643	0.60
	S^-	10.000	0.643	0.90
Masonry 2	E^-	0.000	0.772	0.00
	H^-	1.556	1.870	0.00
	Y^-	3.310	2.338	0.00
	U^-	4.667	0.772	0.60
	S^-	10.000	0.772	0.90
Masonry 3	E^-	0.000	0.324	0.00
	H^-	0.940	0.785	0.00
	Y^-	2.000	0.981	0.00
	U^-	2.820	0.324	0.60
	S^-	10.000	0.324	0.90

and s_c, introduced to represent stiffness recovery under load reversals, as well as on the uniaxial damage variables d_t and d_c, according to Eq. 3.

$$(1-d) = (1-s_t d_c)(1-s_c d_t) \tag{3}$$

To define the damage evolution law, ABAQUS requires the definition of the uniaxial damage variables d_t and d_c. The compressive damage parameter d_c is defined as a function of the inelastic strain $\tilde{\varepsilon}_c^{in}$ (Table 2), while the tensile damage variable d_t is defined as a function of the cracking strain $\tilde{\varepsilon}_t^{ck}$ (Table 3). These strain measures are used to compute the equivalent plastic strain in compression $\tilde{\varepsilon}_c^{pl}$, and the equivalent plastic strain in tension $\tilde{\varepsilon}_t^{pl}$, according to Eqs. 4 and 5. The values of $\tilde{\varepsilon}_c^{pl}$ and $\tilde{\varepsilon}_t^{pl}$ must be always positive and increasing with increasing $\tilde{\varepsilon}_c^{in}$ and $\tilde{\varepsilon}_t^{ck}$.

Table 3 –
CDP parameters in tension adopted for the masonry materials.

Material	Point	Cracking Strain $\tilde{\varepsilon}_t^{ck}$ [‰]	Uniaxial Tensile Stress σ_t [MPa]	Damage in Tension d_t [-]
Masonry 1	E^+	0.000	0.263	0.00
	Y^+	2.483	0.292	0.00
	S^+	10.000	0.175	0.90
Masonry 2	E^+	0.000	0.316	0.00
	Y^+	2.483	0.351	0.00
	S^+	10.000	0.210	0.90
Masonry 3	E^+	0.000	0.132	0.00
	Y^+	1.500	0.147	0.00
	S^+	10.000	0.088	0.90

$$\tilde{\varepsilon}_c^{pl} = \tilde{\varepsilon}_c^{in} - \frac{d_c}{(1-d_c)} \bullet \frac{\sigma_c}{E_0} \tag{4}$$

$$\tilde{\varepsilon}_t^{pl} = \tilde{\varepsilon}_t^{ck} - \frac{d_t}{(1-d_t)} \bullet \frac{\sigma_t}{E_0} \tag{5}$$

In the absence of compressive damage, the equivalent plastic strain in compression is assumed equal to the inelastic strain, i.e. $\tilde{\varepsilon}_c^{pl} = \tilde{\varepsilon}_c^{in}$, while in absence of tensile damage the equivalent plastic strain in tension coincides with the cracking strain, i.e. $\tilde{\varepsilon}_t^{pl} = \tilde{\varepsilon}_t^{ck}$.

6. Modal analysis

This section presents the results of the preliminary modal analysis, discussed in terms of the identified modal shapes and the corresponding effective masses, which are reported in Fig. 7 . The modal analysis was adopted to characterize the global dynamic behaviour, identify the dominant vibration modes and associated mass participation ratios. The obtained modal properties were used to support the interpretation of the seismic response under different incidence angles. It should be noted that the modal analysis was not intended as a calibration or validation procedure, as no experimental dynamic identification data (e.g., measured natural frequencies or mode shapes) were available for comparison. Consequently, the numerical model was defined based on the available geometric, constructional, and mechanical information, consistently with the comparative objective of the study.

The modal analysis provided the first ten natural frequencies of the numerical model, ranging from 6.44 Hz for the first mode to 16.85 Hz for the tenth mode. The cumulative modal participating mass exceeds the commonly adopted threshold of 85% in the X direction after the first two modes, reaching approximately 97.24%, while in the Y direction this threshold is reached after the first three modes, with a cumulative participating mass of approximately 99.59%. Therefore, the first three modes are sufficient to ensure at least 85% mass participation in both principal horizontal directions.

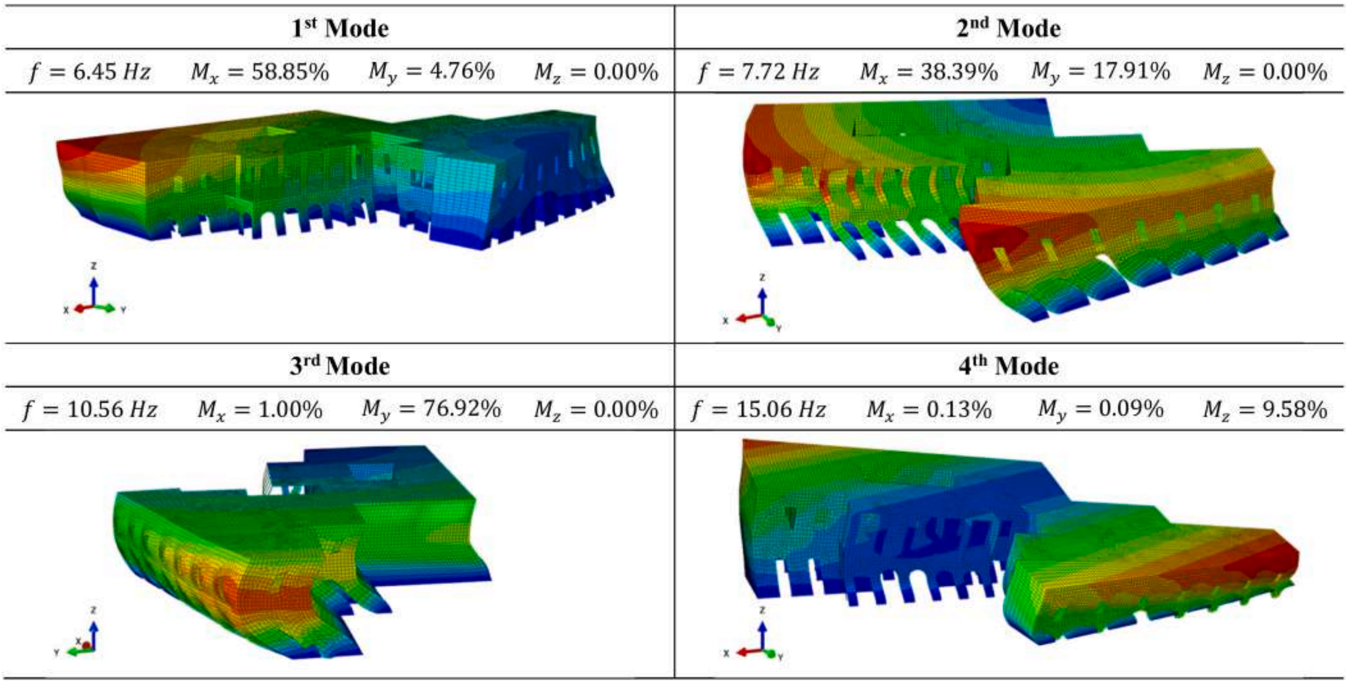

Fig. 7. – Modal shapes obtained for the case study with f frequency, M_x effective mass along the x-direction, M_y effective mass along the y-direction, M_z effective mass along the z-direction.

The linear dynamic behaviour of the building (Fig. 7) is characterised by a first vibration mode that is predominantly translational along the x-direction, a second mode of torsional nature, with coupled displacement components along the two orthogonal directions x e y, and a third mode that is mainly translational along the y-direction. The fourth vibration mode is instead characterised by a predominant translation along the z-direction, associated with oscillations concentrated around the central portion of the building that connects the two main structural bodies. These results indicate that, even in the linear elastic range, the building exhibits markedly irregular dynamic behavior in plan. The modal response is not purely translational along the principal directions, but includes partially uncoupled displacement fields, especially in the higher modes. This suggests that the distribution of mass and stiffness may favor the activation of torsional components during the seismic response. Therefore, the modal analysis provides useful preliminary evidence for interpreting the non-linear results, supporting the need to investigate different incidence angles of the seismic input and their influence on damage distribution and structural capacity.

7. Non-linear quasi-static analyses

The Non-Linear Quasi-Static Analyses are performed in two loading steps. In the first step, the self-weight of the structure is applied through a gravity load along the z-direction. In the second step, the lateral load is applied with a mass-proportional distribution according to a controlled-force procedure, following the directions indicated in Fig. 4e. The results are analysed in terms of forces, displacements and elastic stiffness as functions of both the loading direction and the selected control point, considering the points shown in Fig. 4 f. The control points are defined as follows: CP1 is located at the centroid of the roof of the western structural block (the stiffest part of the aggregate building); CP2 at the global centroid of the roof of the masonry building; CP3 at the centroid of the roof of the eastern structural block (the least stiff part of the aggregate building). The numerical results are examined in terms of base shear by plotting the peak values of V_x, V_y ed V_p as functions of the loading angle θ (Fig. 8a-c), in terms of horizontal displacement of the control nodes by plotting the peak values of U_x, U_y ed U_p as functions of the loading angle θ (Fig. 8d-f) and in terms of elastic stiffness (determined as the ratio between the base shear and the horizontal displacement in the elastic range, namely at the beginning of the load history) measured along the p-direction (K_p) as function of the loading angle θ (Fig. 8 g). It is worth noting that, under conditions of linear elasticity and perfect invariance with respect to load rotation, the plots in Fig. 8a, d would consist of two circles with centres located on the $0^\circ - 180^\circ$ axis and tangent to the $90^\circ - 270^\circ$ axis, the plots in Fig. 8b, e would correspond to the former rotated by 90°. Finally, the plots in Fig. 8c, f, g would consist of circles centred at the origin of the axes. The deviation of V_x and V_y from this ideal behaviour indicates a non-decoupled structural response and, consequently, the presence of torsional effects. The distribution of V_p with varying θ further demonstrates the absence of planimetric isotropy in the structural response, highlighting the existence of preferential directions associated with higher and lower strength. A strong dependence of the structural response on the loading direction also emerges from the analysis of displacement components. Both U_x and U_y exhibit anisotropic behaviour and torsional coupling. In addition, U_p shows a pronounced sensitivity to the loading direction, with a ductility that varies according to the selected control point. In this study, structural ductility is expressed in terms of displacement ductility, defined as $\mu = \Delta u / \Delta y$, where Δu is the ultimate displacement obtained from the capacity curve (displacement registered at the last converging increment of the analysis) and Δy is the displacement corresponding to the conventional yielding point. This definition follows the general formulation proposed by [45], according to which ductility factors are expressed as the maximum deformation divided by the corresponding yield deformation. In terms of elastic stiffness, CP3 is associated with a more isotropic and a less stiff responses compared to the other control points, as confirmed by the more rounded diagram obtained for K_p with increasing loading angle θ (Fig. 8 g).

It is of interest to examine the capacity curves corresponding to the directions associated with maximum and minimum base shear (Fig. 9a),

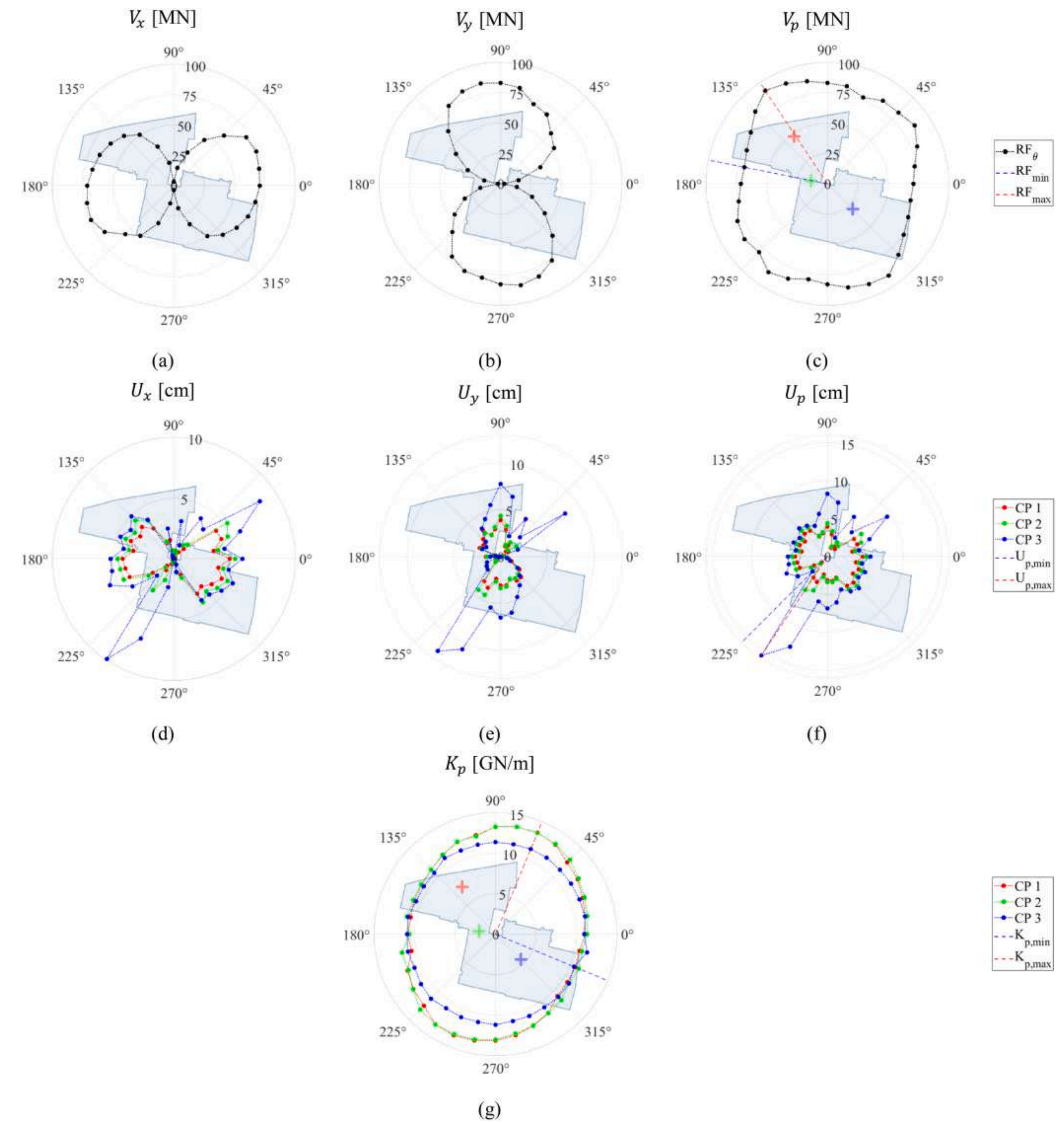

Fig. 8. – Polar diagrams obtained for: (a) peak base shear along the *x*-direction (V_x); (b) peak base shear along the *y*-direction (V_y); (c) peak base shear along the *p*-direction (V_p); (d) displacement along the *x*-direction (U_x) at the peak base shear; (e) displacement along the *x*-direction (U_y) at the peak base shear; (f) displacement along the *p*-direction (U_p) at the peak base shear; (g) elastic stiffness measured along the *p*-direction (K_p).

maximum and minimum horizontal displacement (Fig. 9b), and maximum and minimum elastic stiffness (Fig. 9c). The extreme values of base shear are observed at $\theta = 168.75^\circ$ (minimum value of 69.66 MN) and at $\theta = 123.75^\circ$ (maximum value of 92.07 MN). The minimum horizontal displacement (1 cm) occurs at control point CP1 for $\theta = 225.00^\circ$, whereas the maximum horizontal displacement (21 cm) is attained at control point CP3 for $\theta = 33.75^\circ$. With regard to stiffness, the capacity curves corresponding to Control Points 1 and 2 show a very similar response in the case of maximum stiffness. In contrast, the other capacity curves exhibit comparable overall trends, although differences can be observed in terms of the ultimate displacement attained. It is also worth noting that the minimum stiffness value is substantially independent of the selected control point, whereas the maximum stiffness values obtained for Control Points 1 and 2 are higher than that evaluated for Control Point 3. However, stiffness overall exhibits a limited variability, and a consistent trend can be identified whereby greater stiffness

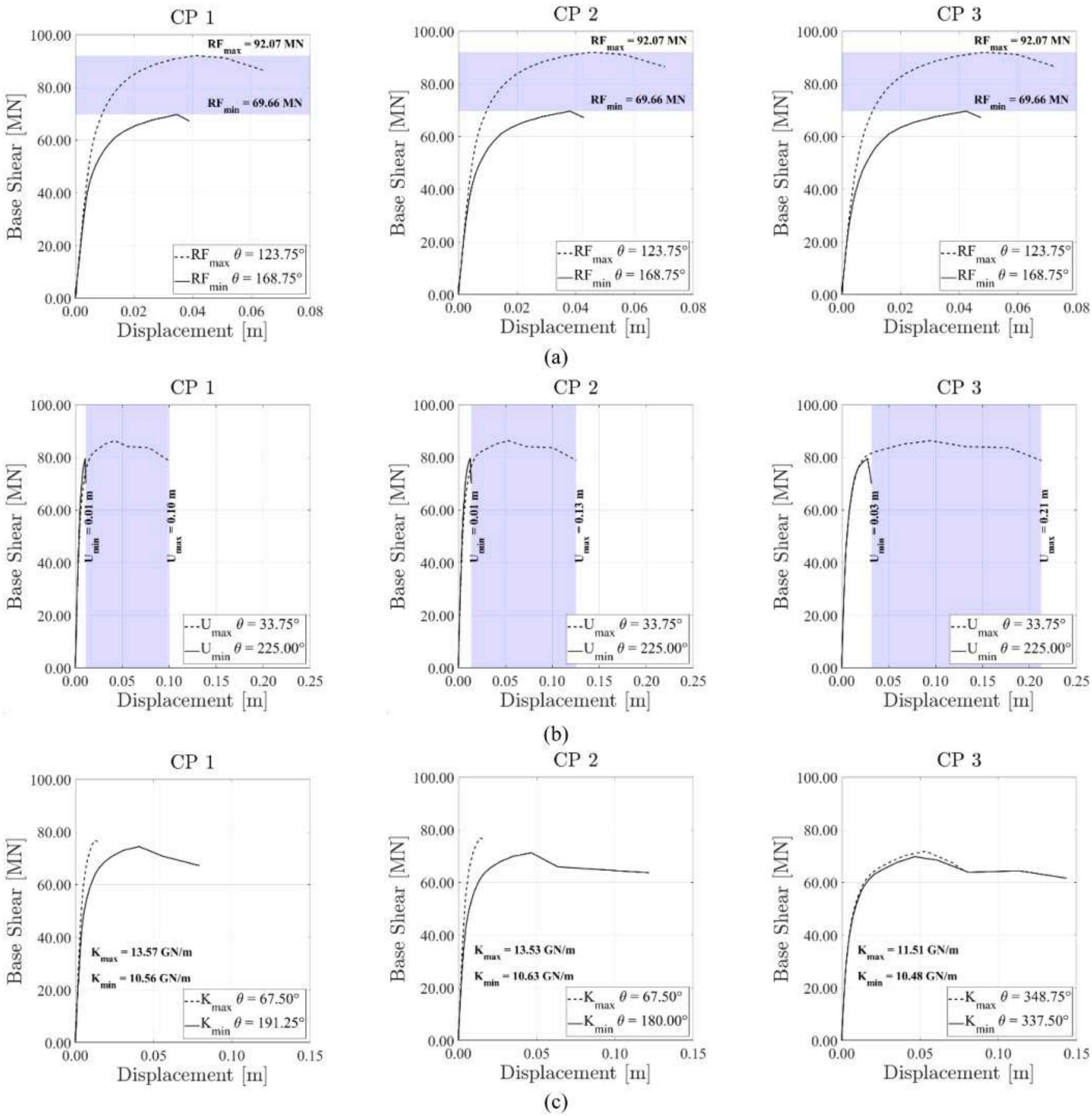

Fig. 9. – Capacity curves corresponding to: (a) minimum and maximum base shear; (b) minimum and maximum horizontal displacement; (c) minimum and maximum elastic stiffness. The shaded rectangle in figure shows: (a) the base shear variability; (b) the horizontal displacement variability.

corresponds to reduced ductility, and vice versa.

An examination of the displacement fields corresponding to the configurations associated with minimum and maximum ductility (Fig. 10a, b) shows that the case $\theta = 33.75^{\circ}$ is characterised by the development of a pronounced torsional motion of the structure, which also results in significant differences among the displacements recorded at the various control points. In this configuration, some portions of the structure reach displacements of up to 35 cm, indicating that selecting the control point in the least stiff area of the building leads to the observation of very large horizontal displacement values and, consequently, to an overestimation of ductility capacity. In contrast, for the configuration associated with minimum ductility, the displacement field is more uniform and the choice of the control point has a negligible influence on the evaluation of ductility.

8. Non-linear dynamic analyses

This section presents the results obtained from the Non-Linear Dynamic Analyses performed using three sets of natural accelerograms. Section 8.1 describes the characteristics of the adopted ground-motion sets, while Section 8.2 reports and discusses the corresponding results.

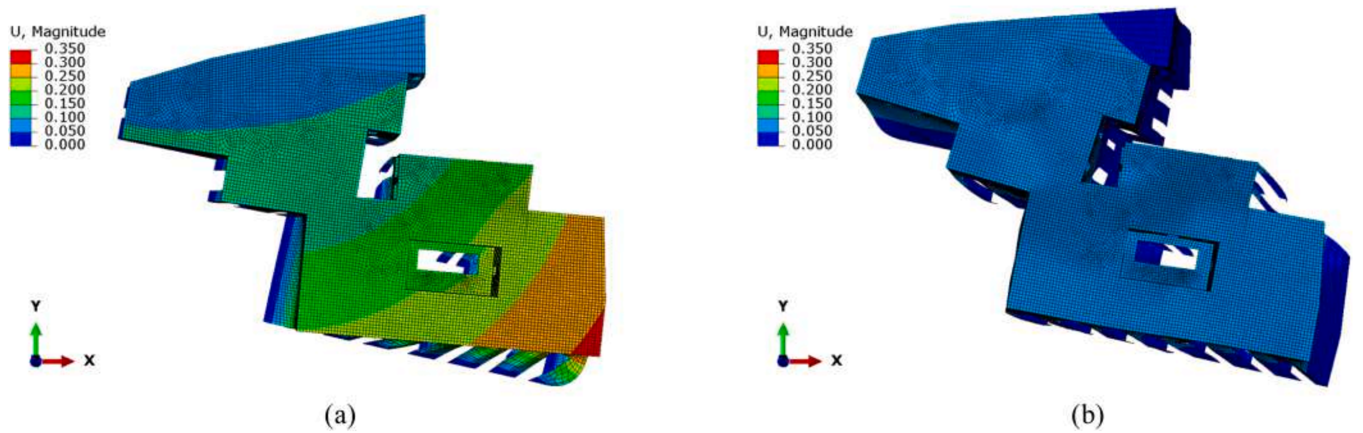

Fig. 10. – Displacement field obtained for the cases: (a) $\theta = 33.75^\circ$ corresponding to the maximum horizontal displacement; (b) $\theta = 123.75^\circ$ corresponding to the maximum base shear.

Table 4 –
Selected ground motions.

ITACA ID	Station	Date/UTC time	Latitude [°]	Longitude [°]	M_L	M_W	R_{epi} [km]	Label
IT−1976–0025	FRC	1976–09–11 16:35:01	46.256	13.233	5.8	5.6	18.6	Friuli 1976
EMSC−20161030_0000029	CIT	2016–10–30 06:40:18	42.838	13.123	5.51	6.6	27.30	Centro-Italia 2016
IT−1997–0006	NCR	1997–09–26 09:40:24	43.031	12.862	5.8	6	10.9	Umbria-Marche 1997

Table 5 –
Selected recording stations and corresponding ground-motion records.

Label	PGA [cm/s^2]			Housner Spectral Intensity [cm]		
	NS	WE	UP	NS	WE	UP
Friuli 1976	−126.7185	−229.3633	−116.0084	21.0230	28.2884	9.4054
Centro-Italia 2016	−209.1729	−319.4734	135.2661	47.0373	63.2964	35.7781
Umbria-Marche 1997	−493.8079	421.7574	408.4845	84.3595	88.2317	76.5686

8.1. Ground motions employed for numerical simulations

Three recorded events (Umbria-Marche 1997, Centro-Italia 2016 and Friuli 1976) are adopted for the Non-Linear Dynamic Analyses. The ground-motion sets are selected so as to exhibit increasing Peak Ground Acceleration (PGA) levels, with the aim of progressively inducing higher stress states in the structure and ultimately leading to collapse. In the numerical analyses, the three components of each ground motions were applied simultaneously, also by considering the vertical component. Details of the selected accelerograms are provided in Table 4, while the corresponding values of PGA, and Housner Spectral Intensity are reported in Table 5. The ground-motion records are extracted using the REXEL software, which allows the selection of three-component waveforms from the ITACA database [46–48]. For clarity of presentation, a label is assigned to each accelerogram set. The acceleration time histories are shown in Fig. 11 and the acceleration response spectra in Fig. 12.

In order to investigate the intrinsic directionality of each accelerogram, a simplified three-dimensional model of a three-degree-of-freedom system, consisting of a fixed-base cantilever with a lumped mass at the free end, was implemented in ABAQUS. The lumped mass is equal to the total mass of the case-study building aggregate, while the stiffness is calibrated so that the natural vibration period matches the first-mode period of the case study. Assuming 5% damping, the system was subjected to the three selected 3D ground motions. The trajectory of the mass, normalised with respect to the maximum displacement, is shown in Fig. 13. The results indicate that the three seismic events have peculiar characteristics with regard to directionality: Umbria–Marche 1997 exhibits predominant seismic excitation along the NS direction with a higher spectral acceleration at 0.155 s along the NS direction; Centro-Italia 2016 is characterized by comparable spectral acceleration along the two directions as evidenced by the uniform trend in the seismic excitation. Finally, Friuli 1976 exhibits a seismic excitation along the two directions WE and NS, as visible from the acceleration spectra.

8.2. Results of non-linear time-history analyses

First, the capability of the implemented numerical model to reproduce the non-linear dynamic structural behaviour is assessed by analysing the results obtained for $\theta = 0^\circ$ and for $\theta = 90^\circ$. To this end, the compressive and tensile damage patterns are examined, together with the time histories of base shear and of the displacements at the control points along the x and y directions. In addition, the resulting hysteretic base shear–displacement relationships are analysed, as well as the evolution of three energy components. For clarity of presentation, these energy terms are labelled according to the notation adopted in the ABAQUS documentation [15]: ALLSE (recoverable elastic strain energy), ALLPD (inelastic dissipated energy, i.e. energy dissipated through inelastic processes such as plasticity), and ALLDMD (energy dissipated by damage).

Since the Concrete Damage Plasticity (CDP) model represents ma-

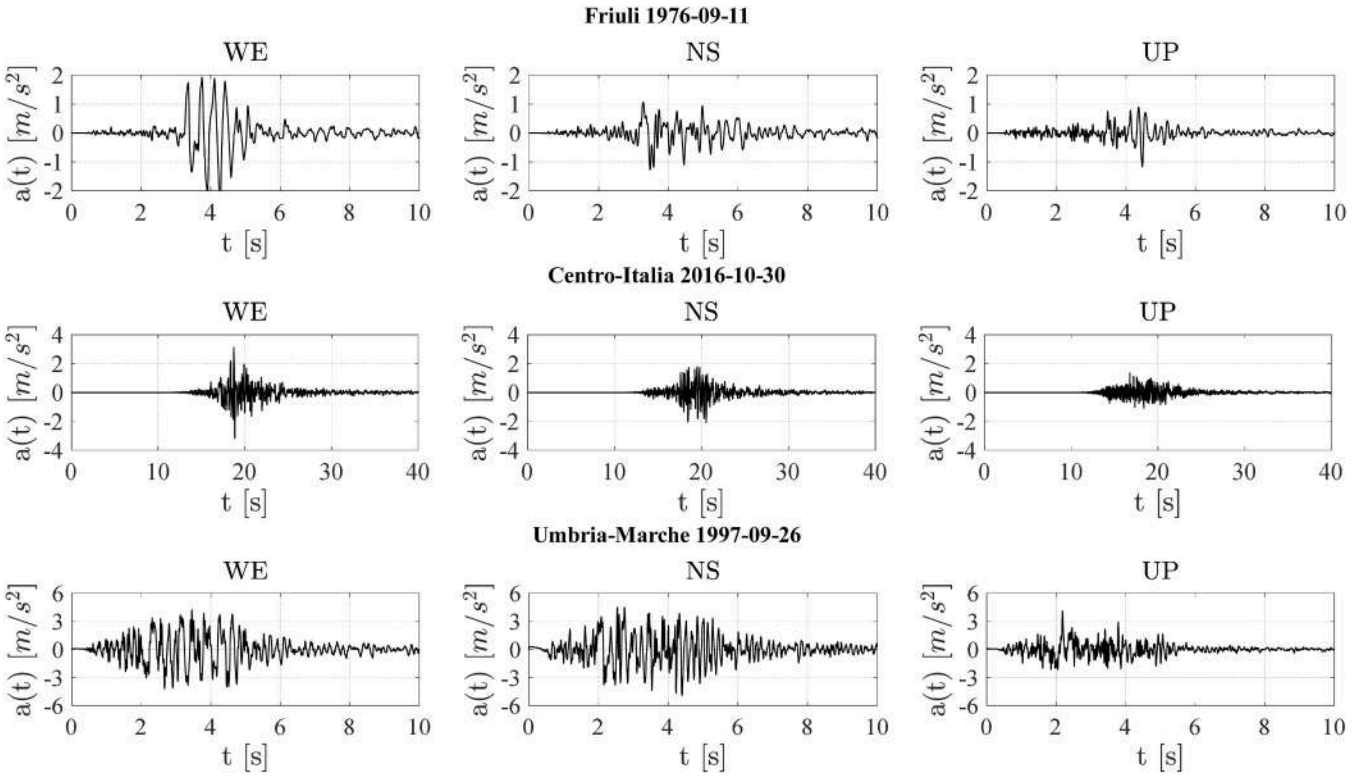

Fig. 11. – Acceleration records of the selected ground-motion sets (Friuli 1976, Centro-Italia 2016, and Umbria–Marche 1997 seismic events).

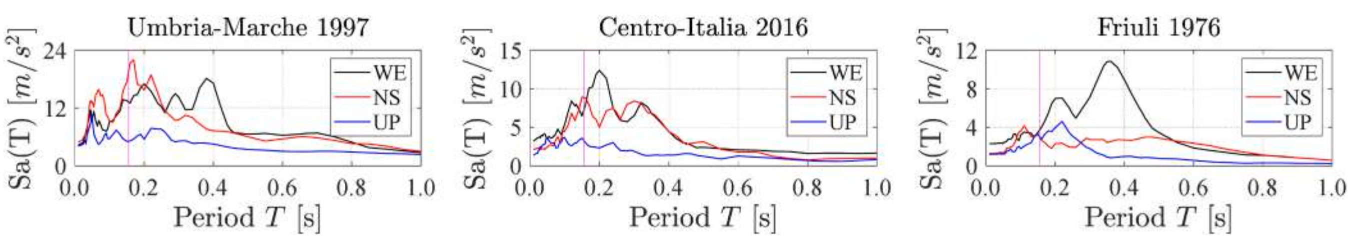

Fig. 12. – Acceleration spectra of the selected ground motion records. In magenta, the oscillator's natural vibration period.

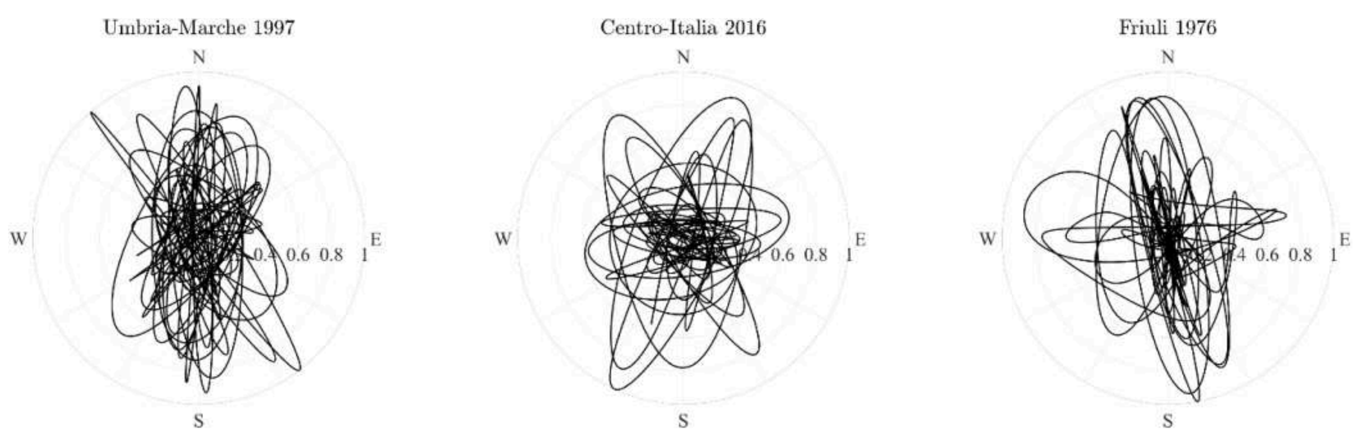

Fig. 13. – Normalized trajectory of a 3DoFs system with a 5% damping subjected to the different ground motion records.

terial degradation through two main mechanisms—tensile cracking and compressive crushing—the tensile and compressive damage maps directly indicate the regions of the building affected by cracking (areas with high values of d_t) and crushing (areas with high values of d_c). The corresponding damage distributions are shown in Fig. 15, according to the viewing directions defined in Fig. 14. It is worth mentioning that for the Umbria-Marche 1997 and Centro-Italia 2016 records, the response histories are not shown over the full duration of the input signals because, in several cases, the numerical analyses reached a collapse condition before the end of the accelerogram. After this stage, the

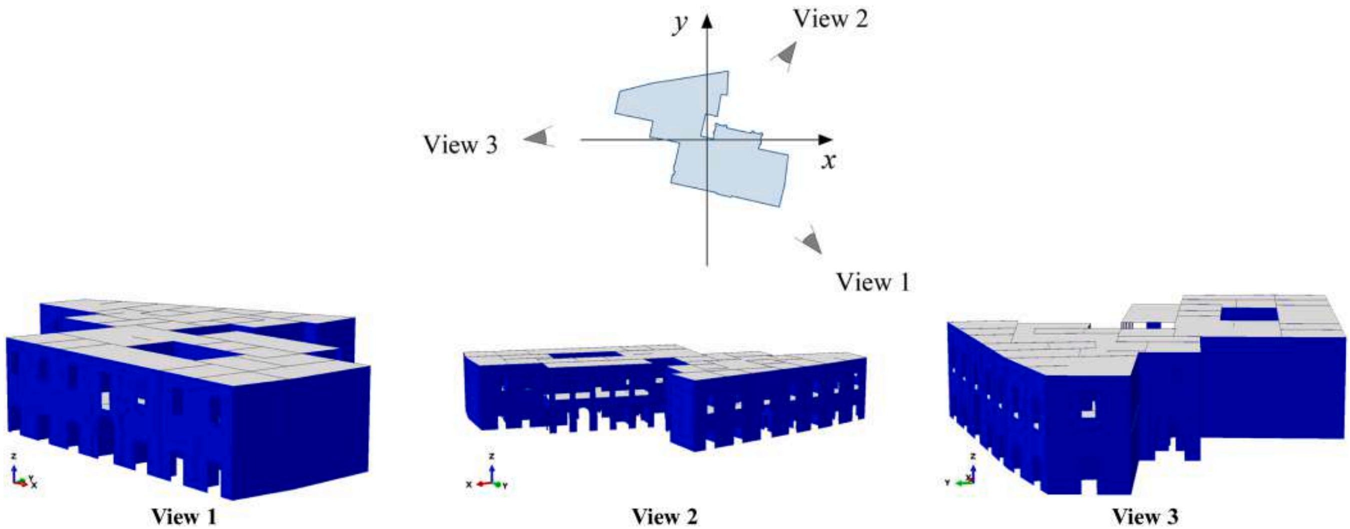

Fig. 14. Reference views used to display tensile and compressive damage distributions.

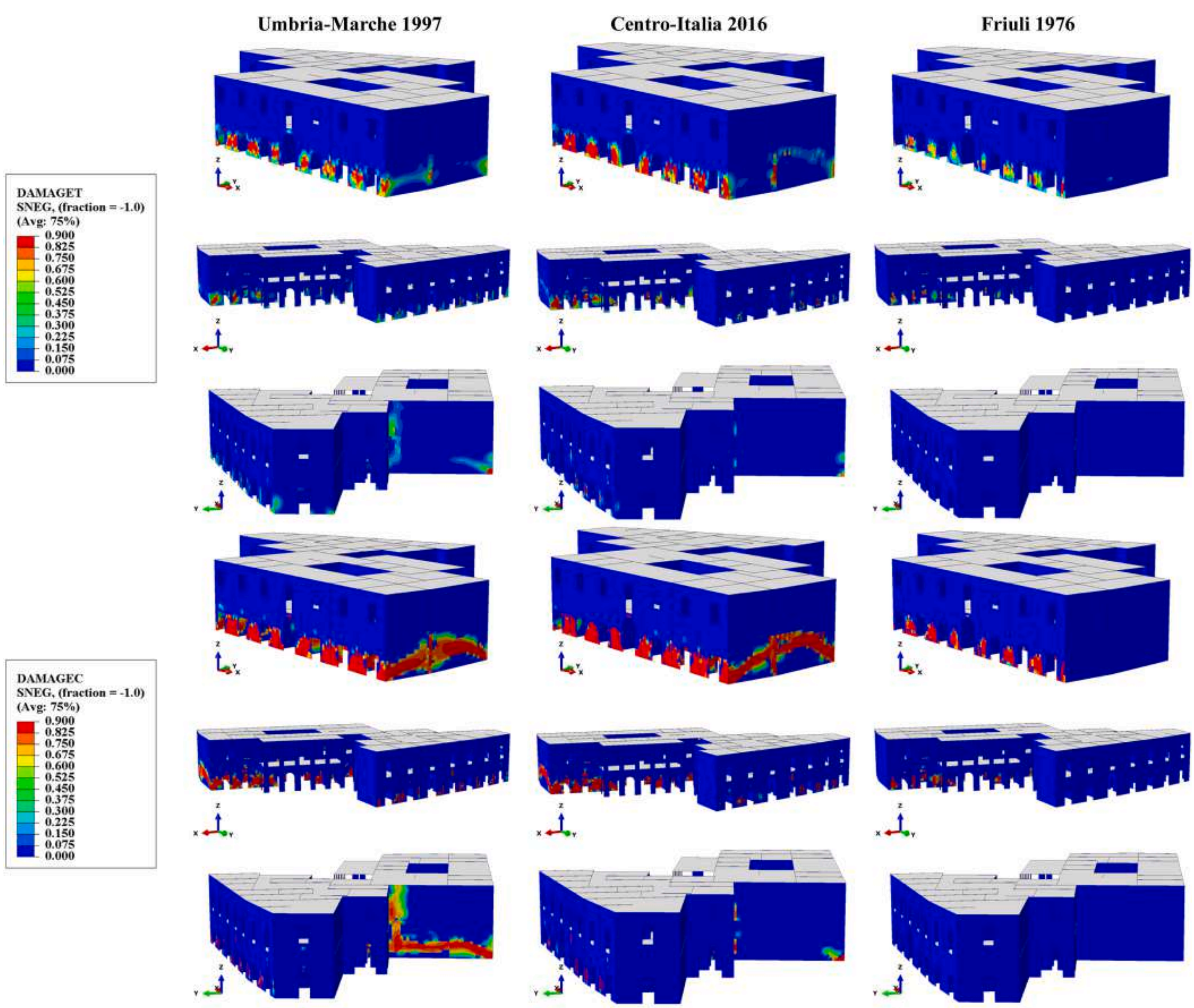

Fig. 15. Tensile and compressive damage maps obtained at the end of the analyses with $\theta = 0^{\circ}$ for the different ground-motion records.

analyses stopped due to lack of convergence, and no further meaningful structural response could be recorded. Therefore, the time histories are reported only up to the last converged increment, which corresponds to the attainment of severe non-linear damage/collapse in the numerical model. Regarding the Friuli 1976 record, collapse was not reached. However, the response histories were intentionally shown over the most relevant time interval, where the significant part of the structural response occurs. This choice was made to improve the readability of the plots and avoid extending the graphs over time intervals characterized by negligible response variations, which would have reduced the clarity of the comparison. Concerning the results for $\theta = 90^\circ$ for the other two records, the detailed time-history plots were reported only for selected representative cases, in order to avoid excessive repetition and maintain the readability of the section. The most severely damaged area is the eastern part of the building, which is characterised by lower stiffness and strength (Masonry 3). Noticeable damage, both in tension and in compression, is also predicted in the zones connecting the two main structural bodies. This response is physically consistent, as out-of-phase vibrations of the two bodies can generate local impact (pounding) effects at their interfaces. The significant compressive damage observed between the base and the first floor might be justified by the presence of a seismic action with a pronounced vertical component. The vertical acceleration may induce transient increases in axial forces in the masonry elements at the lower storeys, thereby promoting compressive damage concentration near the base of the structure.

Considering the Umbria–Marche 1997 ground motion, the time history of the base shear with $\theta = 0^\circ$ (Fig. 16a) shows that, along the x-direction, the shear force oscillates between approximately -50 and $+ 50$ MN, whereas higher values are attained along the y-direction (Fig. 16d). With regard to displacements, peak horizontal displacement values of about -1.5 cm are observed along the x-direction (Fig. 16b) and about $+ 1.5$ cm along the y-direction (Fig. 16e). It is useful to highlight that control point CP3 (located on the roof of the eastern structural block) exhibits, along the x-direction and starting from t = 2 s, an amplification of the displacements associated with localised damage and a change in the natural period (Fig. 16b). A loss of synchronism among the control points becomes evident as a consequence of this period elongation. In particular, the displacement of CP3 reaches a peak out of phase with respect to the other two at t = 3 s. This loss of synchronism may indicate the onset of collapse in the eastern structural block, due to the lower tensile and compressive strength of Masonry 3 compared with Masonry 1 and Masonry 2 (Fig. 15 – left column).

Conversely, along the y-direction, the displacements at the three control points remain comparable throughout the analysis. This behaviour is attributable to the heterogeneous material distribution within the building: seismic excitation along the x-direction promotes larger displacements of the eastern block and induces torsional effects due to the stiffness contrast between the two structural bodies, whereas excitation along the y-direction does not. A similar response pattern is also observed in the results of the pushover analyses.

The hysteretic cycles reported in Fig. 16c, f indicate that, in both horizontal directions, the structure undergoes a progressive degradation of stiffness and strength as the seismic excitation proceeds, accompanied by a significant increase in horizontal displacements. This behaviour is associated with the development of damage in both tension and compression, which leads to a reduction of approximately 90% in the

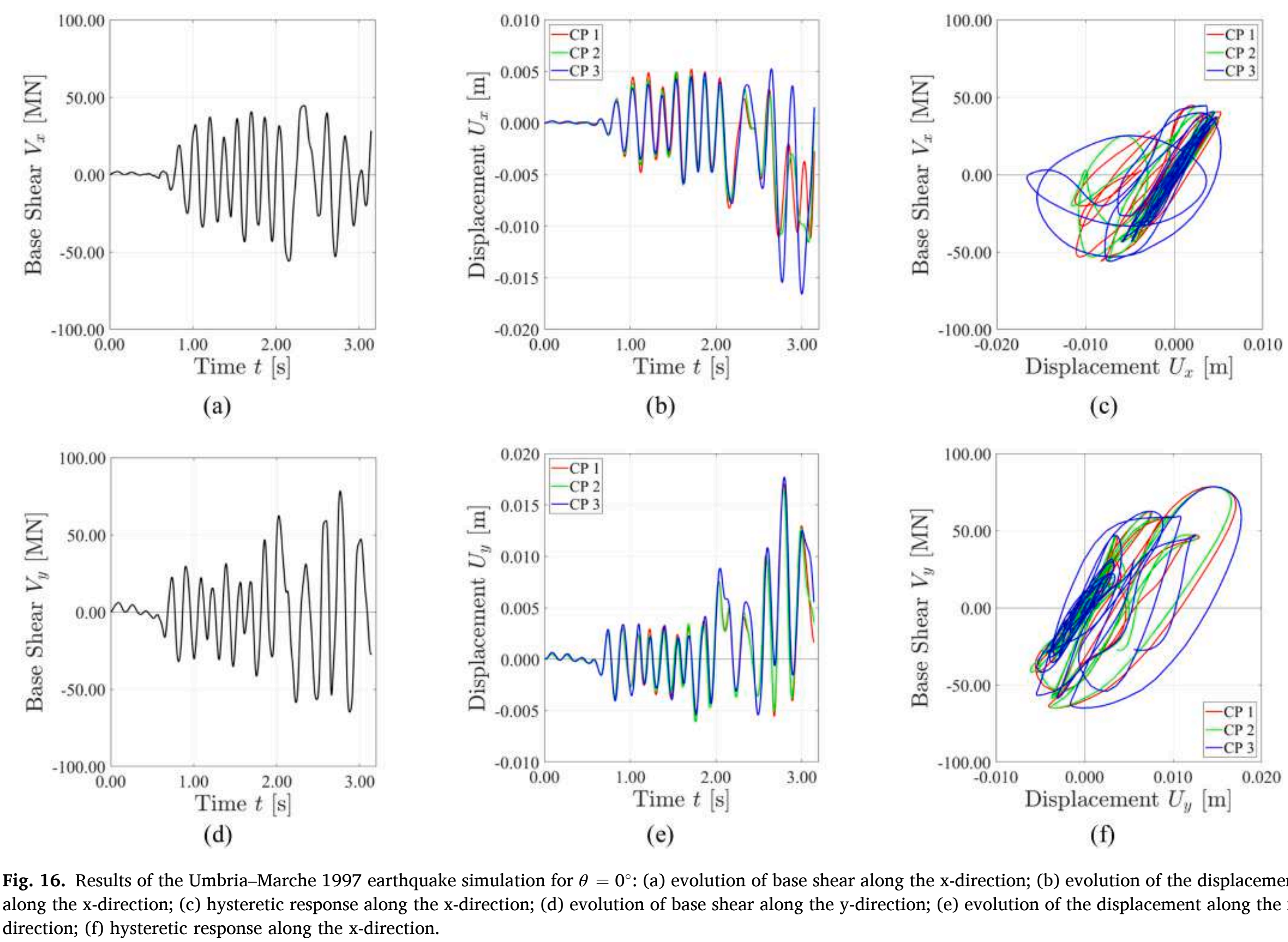

Fig. 16. Results of the Umbria–Marche 1997 earthquake simulation for $\theta = 0^\circ$: (a) evolution of base shear along the x-direction; (b) evolution of the displacement along the x-direction; (c) hysteretic response along the x-direction; (d) evolution of base shear along the y-direction; (e) evolution of the displacement along the x-direction; (f) hysteretic response along the x-direction.

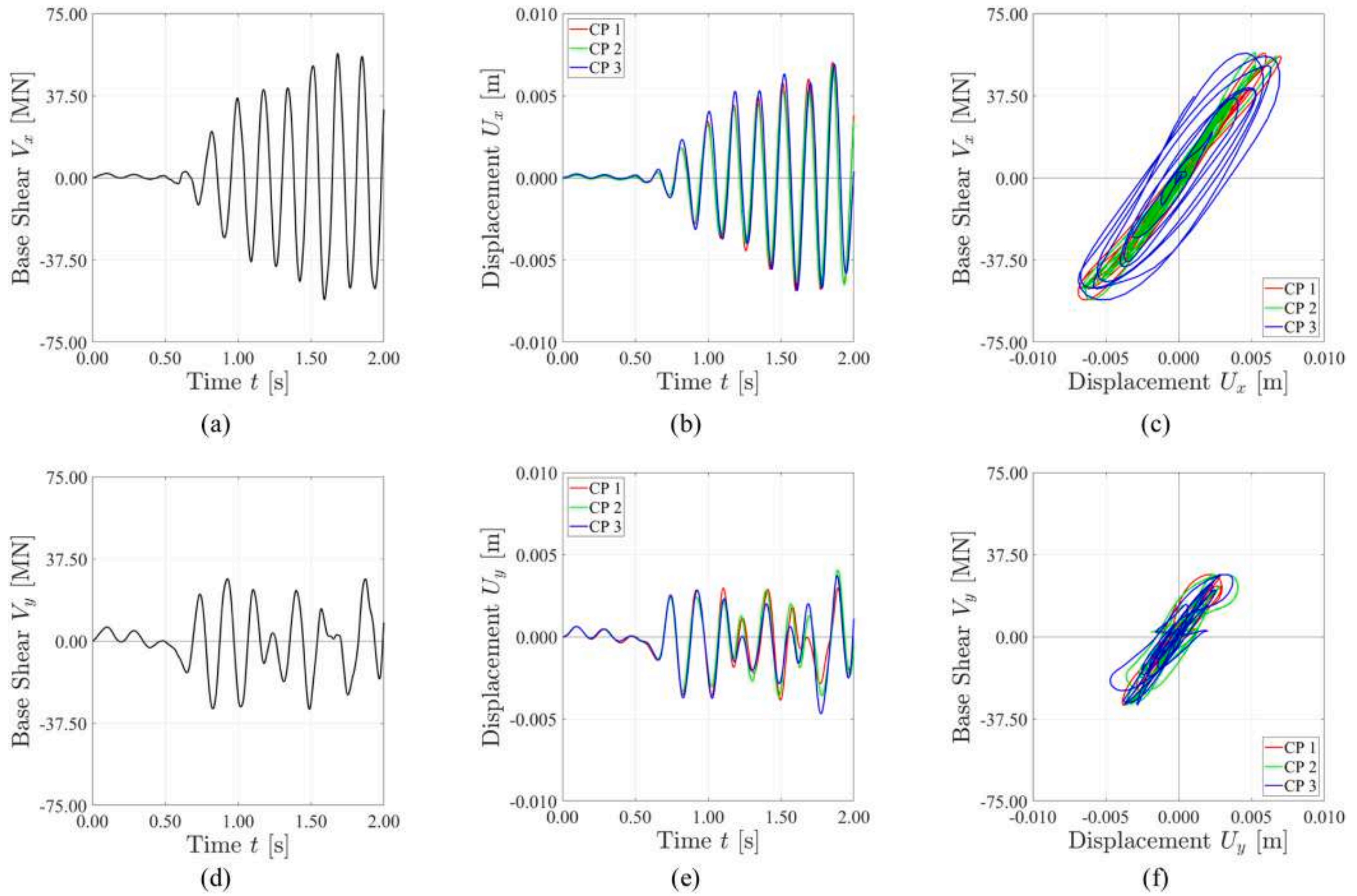

Fig. 17. Results of the Umbria–Marche 1997 earthquake simulation for $\theta = 90^{\circ}$: (a) evolution of base shear along the x-direction; (b) evolution of the displacement along the x-direction; (c) hysteretic response along the x-direction; (d) evolution of base shear along the y-direction; (e) evolution of the displacement along the x-direction; (f) hysteretic response along the x-direction.

elastic stiffness. This effect is markedly more pronounced along the *x*-direction, where the hysteretic loops corresponding to control point CP3 are also wider, indicating a greater amount of energy dissipated through damage in the structural block characterised by Masonry 3.

Examination of the structural response to the Umbria–Marche 1997 accelerogram rotated by $\theta = 90^{\circ}$ shows that, along the x-direction, the base shear force oscillates between approximately -60 and $+60$ MN (Fig. 17a), whereas lower values are recorded along the y-direction (Fig. 17d). With regard to displacements, peak horizontal displacement values of about -0.7 cm are observed along the x-direction (Fig. 17b) and about $+0.5$ cm along the y-direction (Fig. 17e). In this case, after t = 2 s, convergence is lost and the analysis is consequently terminated, due to the attainment of a collapse condition, as confirmed by the presence of extensive structural damage. Also in this case the hysteretic loops corresponding to control point CP3 (Fig. 17 c, f) are wider, indicating a greater amount of energy dissipated through damage in the eastern structural block.

Examination of the dynamic response to the Central Italy 2016 accelerogram rotated by $\theta = 0^{\circ}$ indicates that, along both directions, the base shear force oscillates between approximately -60 and $+60$ MN (Fig. 18a, d). With regard to displacements, peak horizontal displacement values of about 1 cm are observed along the x-direction (Fig. 18b) and about $+0.7$ cm along the y-direction (Fig. 18e). The tendency previously identified is confirmed also in this case, with control point CP3 consistently exhibiting larger displacement demands. After $t = 18$ s, a significant damage state develops in the eastern block. The associated stiffness degradation produces a progressive elongation of the natural period, which in turn leads to a loss of synchronism in the displacements recorded at the control points. Consistently with this interpretation, inspection of the hysteretic cycles reveals, along the x-direction, the same behaviour observed for the Umbria–Marche 1997 record: the loops associated with CP3 are wider, highlighting a greater energy dissipation capacity mobilised through damage in the structural block characterised by Masonry 3 (Fig. 18 c, f).

Analysis of the dynamic behaviour of the building aggregate subjected to the Friuli 1976 accelerogram with an incidence angle of $\theta = 0^{\circ}$ shows that, along the x-direction, the base shear force oscillates between approximately -60 and $+60$ MN (Fig. 19a), whereas lower values are attained along the y-direction (Fig. 19d). With regard to displacements, peak horizontal displacement values of about -0.8 cm are observed along the x-direction (Fig. 19b) and about $+0.3$ cm along the y-direction (Fig. 19e). Also in this case, despite the lower intensity of the input motion, a loss of synchronism in the displacements recorded at the control points is observed after $t = 4$ s. This behaviour is symptomatic of damage development and of a modification of the dynamic properties, with a variation of the natural period primarily affecting the eastern block.

From an energy perspective (Fig. 20) the recoverable elastic strain energy, which is initially non-zero due to the application of self-weight, exhibits oscillations during the analysis but remains a minor contribution to the overall energy balance. This behaviour is consistent with the brittle or quasi-brittle response of masonry, which is inherently unable to store significant amounts of energy in elastic form. The inelastically dissipated energy (ALLPD) represents the dominant component of the system energy balance, in agreement with the development of wide hysteretic loops capable of dissipating substantial energy (Figs. 16–19). In contrast, the energy dissipated through damage (ALLDMD) is comparatively small. This contribution depends directly on the

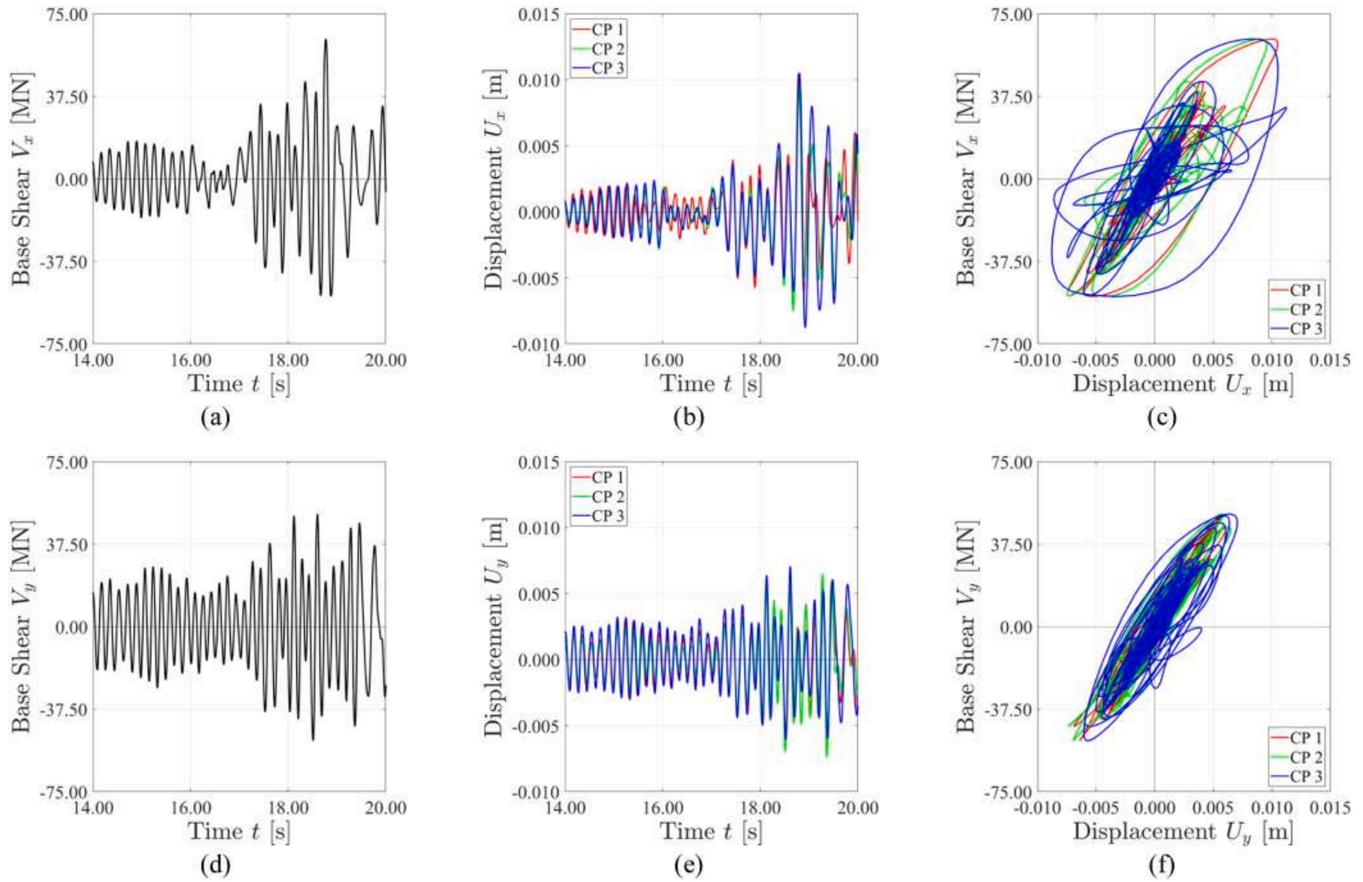

Fig. 18. Results of the Centro-Italia 2016 earthquake simulation for $\theta = 0°$: (a) evolution of base shear along the x-direction; (b) evolution of the displacement along the x-direction; (c) hysteretic response along the x-direction; (d) evolution of base shear along the y-direction; (e) evolution of the displacement along the x-direction; (f) hysteretic response along the x-direction.

definition of the damage variables d_t and d_c as functions of the inelastic strain measures. The limited amount of energy dissipated by damage is attributed to the fact that d_t and d_c are not defined in the strain range between the points Y + and Y- of the constitutive relationship. Within this strain interval, the material develops hysteretic cycles and dissipates energy through inelastic deformation; however, since no damage evolution is prescribed in this range, no damage accumulation occurs and, consequently, no energy dissipation associated with damage is produced.

The results of the Non-Linear Dynamic Analyses (Figs. 21, 22, and 23) are evaluated in terms of base shear (V_m), control-point horizontal displacement (U_m), and control-point acceleration (A_m), computed according to Eqs. 6, 7 and 8.

$$V_m(t,\theta) = \sqrt{V_\xi(t,\theta)^2 + V_\eta(t,\theta)^2} \tag{6}$$

$$U_m(t,\theta) = \sqrt{U_\xi(t,\theta)^2 + U_\eta(t,\theta)^2} \tag{7}$$

$$A_m(t,\theta) = \sqrt{A_\xi(t,\theta)^2 + A_\eta(t,\theta)^2} \tag{8}$$

It can be observed that the dependence of base shear on the incidence angle θ generally exhibits greater variability as the Peak Ground Acceleration (PGA) of the seismic input increases. For the Central Italy 2016 and Friuli 1976 ground motions (Figs. 22a and 23a), the base shear—both in terms of its components and its resultant—shows a certain periodic trend, suggesting a weakly anisotropic structural behaviour just when forces are considered, as already highlighted in Fig. 8c. This pattern is not observed for the Umbria–Marche 1997 ground motion (Fig. 21a), for which the distribution of $V_m(\theta)$ appears almost random. In this case, $\theta = 90°$ emerges as the most critical incidence angle, corresponding to the lowest structural resistance.

With regard to displacements, the results for the Central Italy 2016 and Friuli 1976 ground motions (Figs. 22b and 23b) exhibit a certain symmetry and periodicity in the distribution of ultimate displacements for all control points. This behaviour is not observed in the case of the Umbria–Marche 1997 ground motion (Fig. 21b), for which the displacement patterns appear more irregular. Concerning the influence of the selected control point, CP3 is generally associated with larger displacements. Floor accelerations display a marked dependence on the incidence angle θ only for the Umbria–Marche 1997 ground motion (Fig. 21c), whereas a limited sensitivity to the loading direction is observed for the Central Italy 2016 and Friuli 1976 records (Figs. 22c and 23c). In this case, CP3 does not systematically exhibit higher accelerations than the other control points, and mixed response patterns are observed.

With the aim of investigating the variability of base shear and peak horizontal displacement obtained from Non-Linear Dynamic Analyses as a function of the selected control point, Fig. 24 presents the horizontal displacement-base shear pairs derived from each analysis for the different control points adopted. Three convex envelopes are constructed from these points in order to appraise the existing variability in both the peak base shear and the maximum horizontal displacement attained in the dynamic simulations. The interpretation of Fig. 24 shows that adopting control point CP1 systematically leads to an underestimation of the maximum horizontal displacement, whereas adopting CP3 consistently results in an overestimation.

Although control point CP2 is adopted in accordance with code provisions and provides an intermediate estimate of the global structural

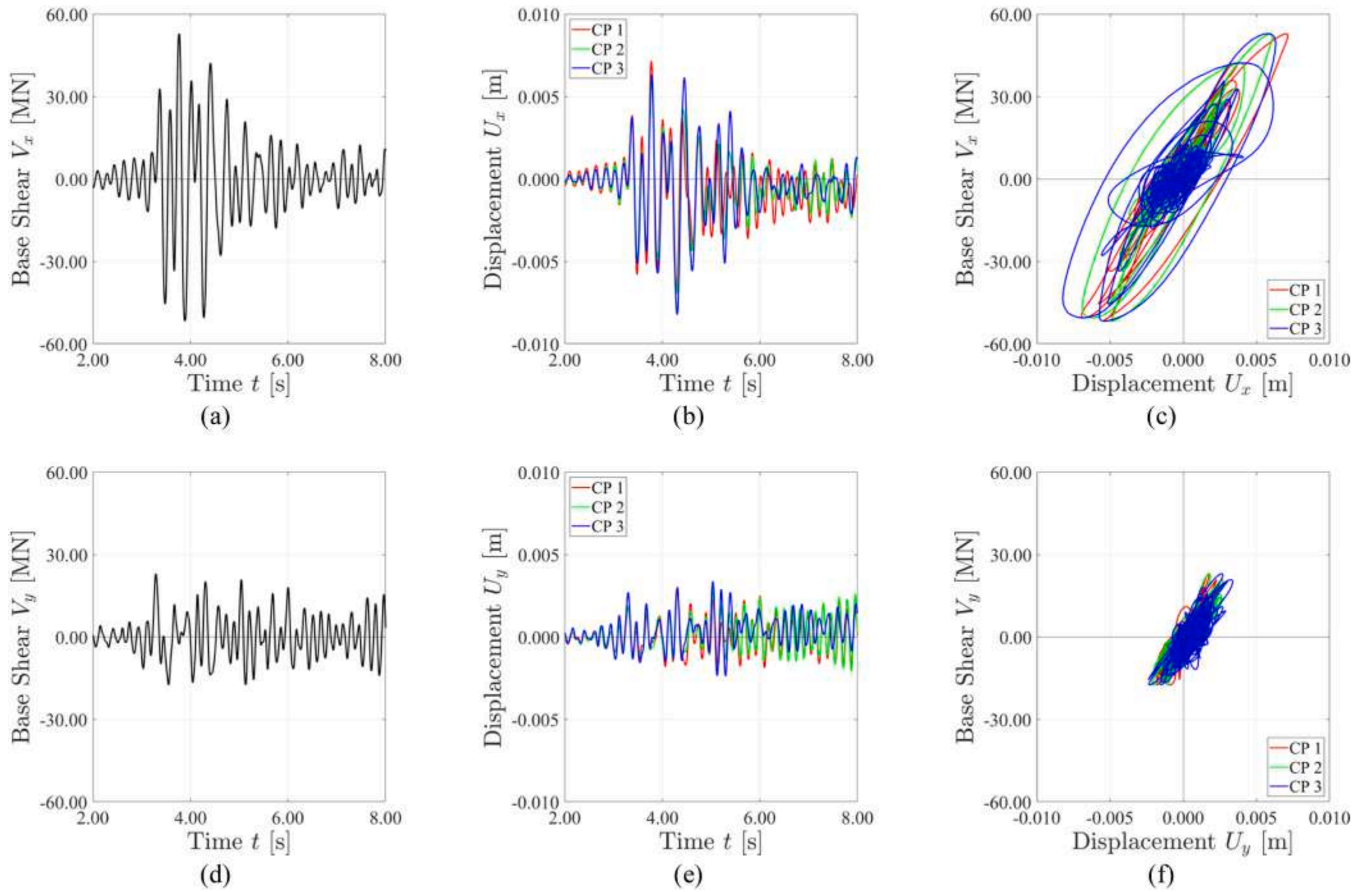

Fig. 19. Results of the Friuli 1976 earthquake simulation for $\theta = 0°$: (a) evolution of base shear along the x-direction; (b) evolution of the displacement along the x-direction; (c) hysteretic response along the x-direction; (d) evolution of base shear along the y-direction; (e) evolution of the displacement along the x-direction; (f) hysteretic response along the x-direction.

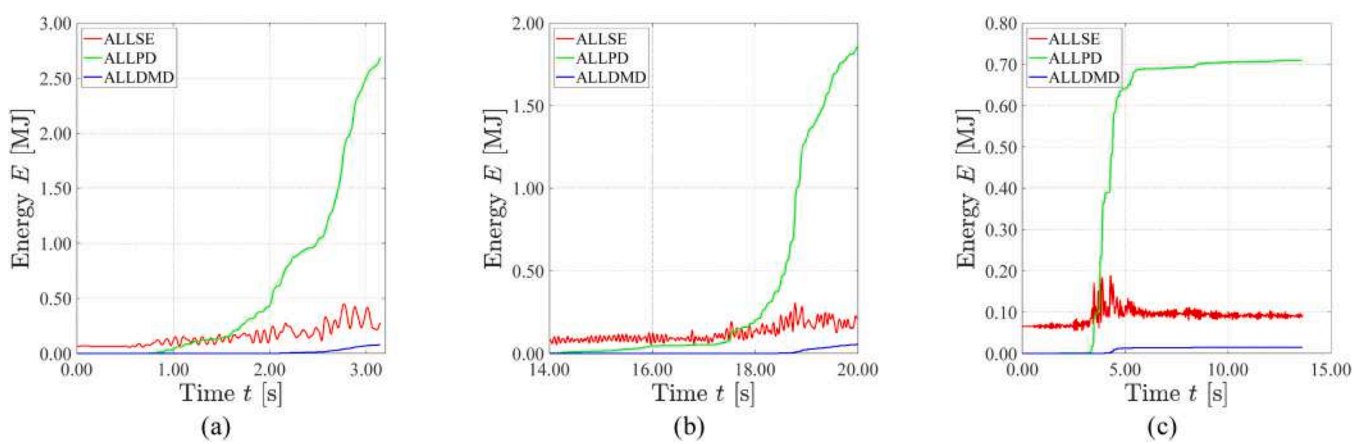

Fig. 20. Energy dissipation for the different ground-motion records with $\theta = 0°$: (a) Umbria–Marche 1997; (b) Central Italy 2016; (c) Friuli 1976.

response, its representativeness may be limited for building aggregates characterised by pronounced spatial heterogeneity of mechanical properties and subjected to ground motions with intrinsic directionality. In such conditions, the governing demand tends to migrate toward the portions of the structure where stiffness degradation localises, while torsional effects and record directionality may further amplify the response at specific blocks. Within the analysed cases, CP2 systematically provides an intermediate estimate of peak horizontal displacement, whereas the maximum demand is often attained in the eastern block, where the weaker Masonry 3 material promotes earlier damage, period elongation, and subsequent phase desynchronisation. Consequently, the use of CP2 alone may lead to a non-conservative evaluation of local deformation demand, and it should be interpreted primarily as a global response indicator rather than as a predictor of the most critical condition within the aggregate.

In addition, the spread of the convex envelopes indicates that, for the cases examined, increasing earthquake intensity is associated with greater variability in the predicted response.

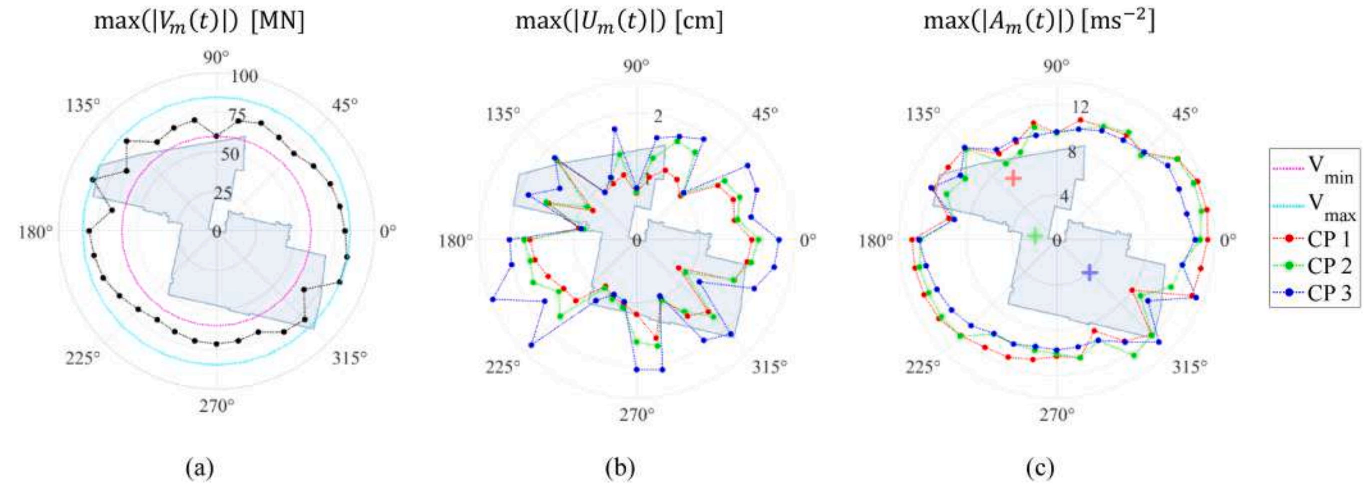

Fig. 21. – Polar diagrams obtained for Umbria-Marche 1997 earthquake varying rotation angle θ of the auxiliary reference system $\{O, \xi, \eta, z\}$ with respect to the fixed reference system: (a) max(|$V_m(t)$|); (b) max(|$U_m(t)$|); (c) max(|$A_m(t)$|).

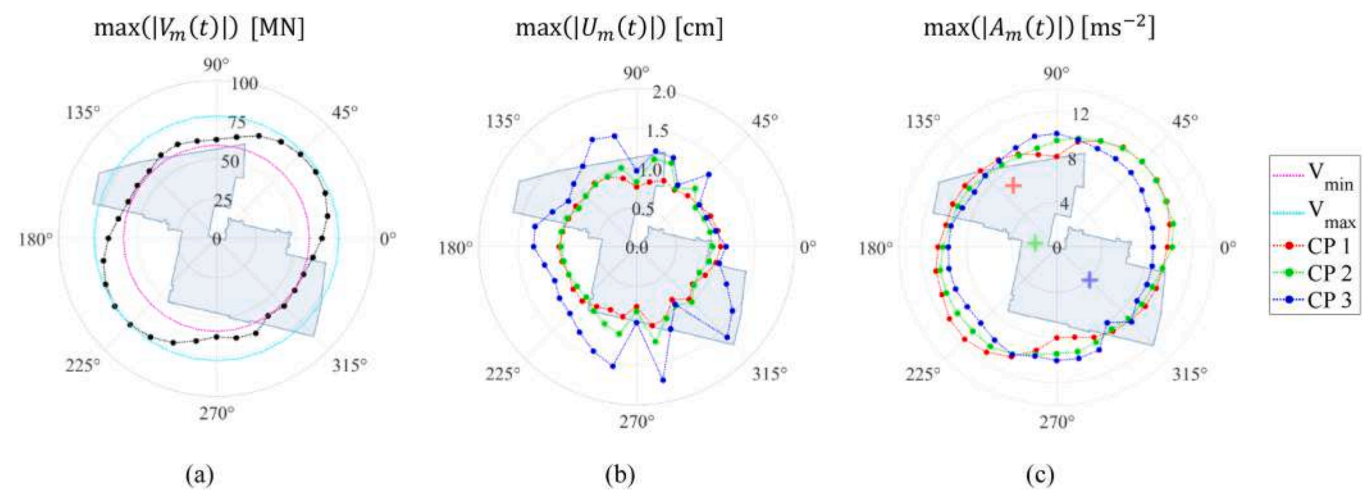

Fig. 22. – Polar diagrams obtained for Centro-Italia 2016 earthquake varying rotation angle θ of the auxiliary reference system $\{O, \xi, \eta, z\}$ with respect to the fixed reference system: (a) max(|$V_m(t)$|); (b) max(|$U_m(t)$|); (c) max(|$A_m(t)$|).

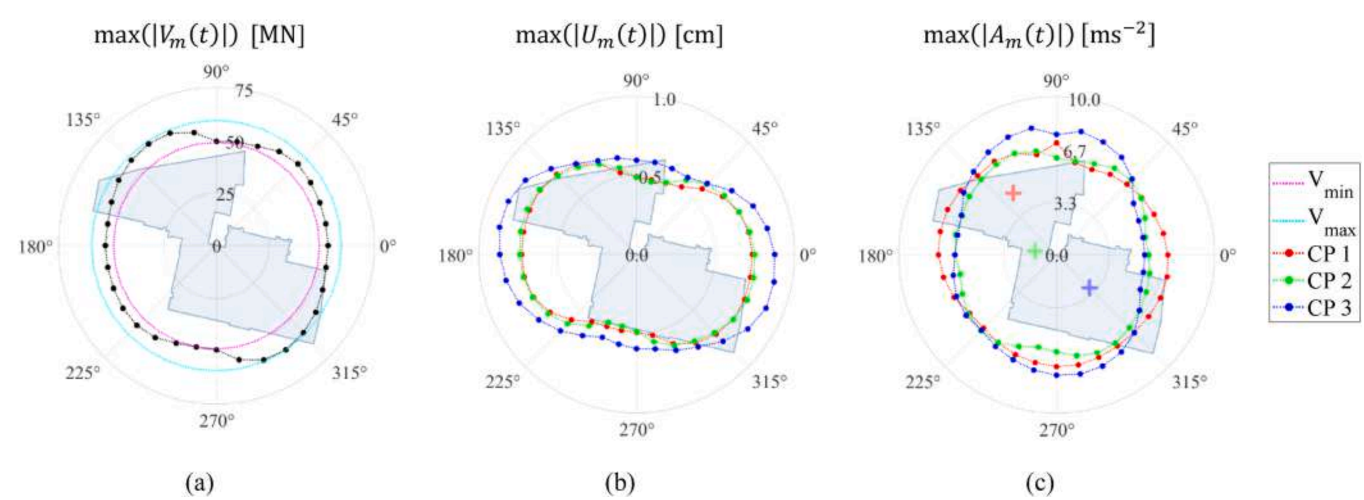

Fig. 23. – Polar diagrams obtained for Friuli 1976 earthquake varying rotation angle θ of the auxiliary reference system $\{O, \xi, \eta, z\}$ with respect to the fixed reference system: (a) max(|$V_m(t)$|); (b) max(|$U_m(t)$|); (c) max(|$A_m(t)$|).

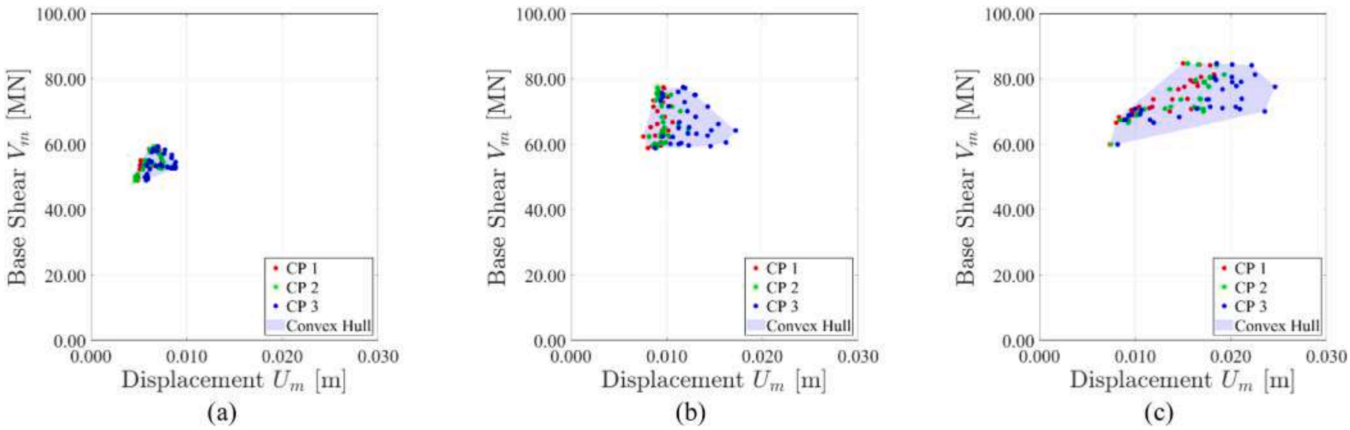

Fig. 24. Horizontal displacement-base shear points obtained from dynamic analyses adopting different control points and different earthquake registrations: (a) Friuli 1976; (b) Centro-Italia 2016; (c) Umbria-Marche 1997.

9. Comparison between quasi-static and dynamic analyses

In order to compare the results of the pushover analyses with those obtained from the non-linear dynamic simulations, Fig. 25 superimposes the envelopes of the horizontal displacement–base shear maps derived for the Friuli 1976, Central Italy 2016, and Umbria–Marche 1997 ground motions onto the capacity curves. This comparison is carried out while accounting for the differences in the structural response associated with the various control points.

The comparison presented in Fig. 25 shows that pushover and Non-Linear Dynamic Analyses provide similar peak base shear values, with the latter progressively increasing with the PGA of the adopted ground motion. The quasi-static simulations lead to peak base shear values ranging approximately between 70 and 90 MN. The dynamic analyses return base shear demands between 49 and 60 MN for the Friuli 1976 earthquake, between 59 and 77 MN for Central Italy 2016, and between 60 and 85 MN for Umbria–Marche 1997. Therefore, for a given horizontal displacement level, the variability of the base shear predicted by pushover analyses is generally larger than that obtained from non-linear dynamic simulations.

With reference to structural ductility, the pushover analyses predict collapse horizontal displacements ranging between 1 cm and 21 cm. The dynamic simulations provide maximum horizontal displacement values between 5 and 9 mm for Friuli 1976, between 7 and 17 mm for Central Italy 2016, and between 7 and 25 mm for Umbria–Marche 1997. Hence, for a given base shear, the dispersion of horizontal displacement obtained from pushover analyses is again wider than that derived from Non-Linear Dynamic Analyses.

Regarding the reduced ductility observed in the Non-Linear Dynamic simulations, Casolo & Uva [49] noted that dynamic loading conditions may activate local collapse mechanisms that do not develop under quasi-static loading. In particular, dynamic analyses tend to excite higher-frequency modes associated with local structural responses, whereas Non-Linear Quasi-Static Analyses predominantly induce a global deformation pattern that may not be fully representative of the structural behaviour under seismic excitation. This occurrence is confirmed by the damage maps (Fig. 15), which show the development of damage concentrated in limited portions of the building aggregate rather than the more distributed pattern typically resulting from a quasi-static action.

On the basis of the obtained results, it can be stated that, although pushover analysis is capable of highlighting the anisotropy of the structural response, it does not always identify the same weakest and strongest directions obtained from Non-Linear Dynamic Analyses. This discrepancy is not unexpected, since Non-Linear Static Analyses mainly describe the intrinsic directional dependence of the structural capacity under monotonically increasing lateral loads, whereas dynamic analyses also account for the intrinsic directionality and time-dependent nature of earthquake ground motions. This directionality manifests in natural accelerograms through pulses acting along different orientations, occurring at different times, and characterized by distinct spectral contents. As a consequence, the directions associated with maximum or minimum response in the dynamic analyses may differ from those identified by the pushover curves. Non-Linear Dynamic Analyses are therefore essential to capture the combined effect of structural anisotropy and record-dependent features, whereby different inputs may

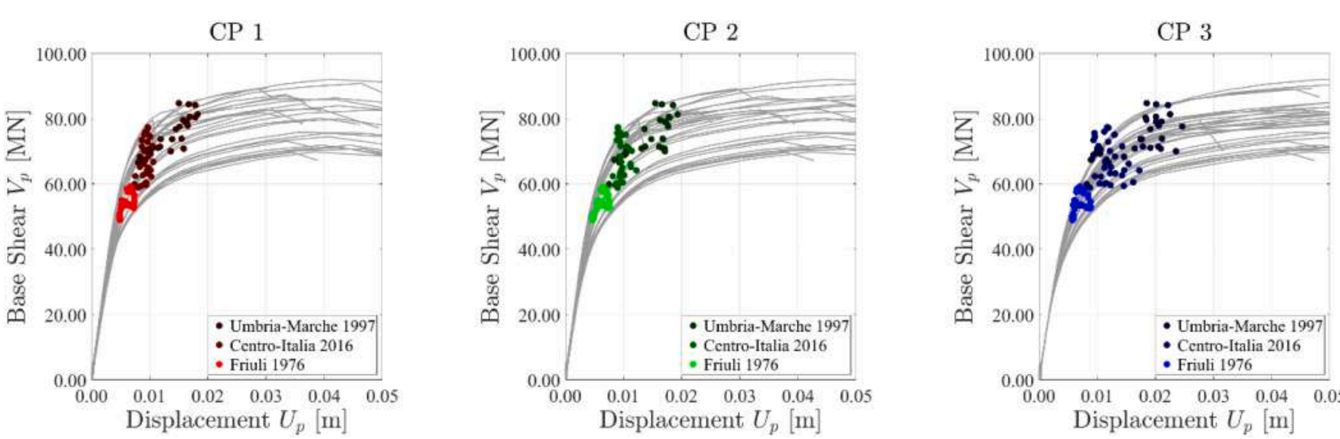

Figure. 25. Comparison between numerical pushover capacity curves and dynamic convex hulls obtained adopting different control points.

selectively activate specific modal responses, trigger local softening, and ultimately shift the location and magnitude of peak demand.

For the Friuli 1976, Central Italy 2016, and Umbria–Marche 1997 recordings, as already shown in Figs. 11–13, pulses are observed in different directions and with markedly different spectral contents, resulting in significant discrepancies between the west-east and north–south components. The interaction between these pulses and the strongly anisotropic features of the building aggregate considered as case study may lead to premature collapse when the direction of maximum impulse coincides with the direction of minimum resistance. Conversely, if the strongest impulse acts along the direction of greater strength, the structural capacity may be overestimated, as discussed by Casolo [50]. Since the incidence angle at which the direction of maximum impulse aligns with the weakest structural direction cannot be known a priori, it is essential in professional assessment practice to evaluate the response by rotating the adopted seismic input. This strategy alone enables identification of the most unfavourable incidence angle and prevents potentially severe overestimations of structural resistance under seismic actions.

10. Final remarks and future developments

This study investigated the effects of structural response anisotropy and of the selected control point on the evaluation of Engineering Demand Parameters (EDPs) for existing masonry aggregate buildings characterised by irregular geometry and a heterogeneous spatial distribution of structural element strength. Both Non-Linear Quasi-Static and Non-Linear Dynamic Analyses were performed. In existing masonry constructions, the spatial variability and directionality of seismic action associated with the angle of incidence relative to the structure represents a dominant source of uncertainty that must be carefully modelled. This variability, combined with the specific geometric configuration of the building and the spatial distribution of stiffness and strength, may lead to an unpredictable structural response that we recommend to explicitly consider in safety assessments. Consequently, structural response anisotropy plays a key role in the seismic assessment of masonry buildings, as it can significantly affect the determination of safety factors under horizontal actions.

Using Palazzo Carmelo, a historic aggregate building located in Cerignola (Apulia, Italy) and documented in the literature, as a case study, the structural behaviour was analysed through 32 Non-Linear Quasi-Static Analyses and 96 Non-Linear Dynamic Analyses, varying the loading direction and considering different control points and different EDPs. An advanced Finite Element model was developed in ABAQUS, adopting the Concrete Damage Plasticity model to represent the post-elastic behaviour of the materials identified through in-situ investigations.

The main findings of the study can be summarised as follows:

- Structural response is markedly anisotropic, with strength, stiffness, and displacement demand strongly dependent on the direction of seismic incidence.
- The spatial distribution of stiffness and strength significantly influences the evaluation of ductility and displacement demand, making the choice of control point a critical modelling assumption.
- Among the examined EDPs, floor acceleration is the least affected by control-point location, whereas horizontal displacement-based measures are highly sensitive to both loading direction and control-point selection.
- Non-Linear Quasi-Static Analyses are effective in identifying preferential weak directions, but they tend to overestimate ductility compared to Non-Linear Dynamic Analyses and cannot account for the intrinsic directionality of seismic motion.
- Non-Linear Dynamic Analyses reveal a more complex and less predictable response, particularly for stronger ground motions, due to the activation of torsional effects and local mechanisms. Moreover, the use of natural accelerograms in Non-Linear Dynamic Analyses allows the combined effects of structural anisotropy and seismic directionality to be modelled, which is due to the presence of impulses in different directions, times and frequencies.

Future developments of this work will focus on the investigation of structural response anisotropy in masonry buildings under complex aggregation conditions, explicitly accounting for contact and interaction between adjacent structural units. To this end, the interaction between neighbouring buildings will be modelled through interface springs governed by elasto-plastic constitutive laws, allowing changes in stiffness, strength, and ductility induced by structural contact to be simulated. Extensive parametric analyses will be carried out to assess how inter-building interaction influences the seismic response of masonry structures within aggregates.

CRediT authorship contribution statement

Siro Casolo: Conceptualization, Methodology, Supervision, Writing – review & editing. **Luigi Salvatore Rainone:** Data curation, Formal analysis, Investigation, Methodology, Visualization, Writing – original draft, Writing – review & editing. **Elisa Bertolesi:** Conceptualization, Data curation, Methodology, Supervision, Writing – original draft, Writing – review & editing. **Giuseppina Uva:** Conceptualization, Methodology, Supervision, Writing – review & editing.

Declaration of Competing Interest

The authors declare the following financial interests/personal relationships which may be considered as potential competing interests: Elisa Bertolesi serves as an Associate Editor of Structures. She also served as Lead Guest Editor of the Special Issue Advances in the Design and Simulation of Masonry Infilled Structures under Extreme Loads (2022).

Acknowledgments

Luigi Salvatore Rainone acknowledges the financial support by the PhD fellowship funded by the European Union – NextGenerationEU, under the National Recovery and Resilience Plan (PNRR), Mission 4 “Education and Research” (D.M. 118/2023), CUP: D93C23000430005.

Giuseppina Uva acknowledges the financial support by FABRE - “Research consortium for the evaluation and monitoring of bridges, viaducts and other structures” (www.consorziofabre.it/en). Any opinion expressed in the paper does not necessarily reflect the view of the funder.

Conflicts of Interest

The authors declare that they have no conflicts of interest.

References

[1] Feliciano D, Arroyo O, Carrillo J, Liel AB, Murray PB. Framework to assess the seismic performance of non-engineered masonry infilled RC frame buildings accounting for material uncertainty (April). Structures, 50. Elsevier; 2023. p. 1191–203. https://doi.org/10.1016/j.istruc.2023.02.100 (April).

[2] Gonen S, Pulatsu B, Erdogmus E, Lourenço PB, Soyoz S. Effects of spatial variability and correlation in stochastic discontinuum analysis of unreinforced masonry walls. Constr Build Mater 2022;337:127511. https://doi.org/10.1016/j.conbuildmat.2022.127511.

[3] Puncello I, Caprili S. Seismic assessment of historical masonry buildings at different scale levels: a review. Appl Sci 2023;13(3):1941. https://doi.org/10.3390/app13031941.

[4] Rota M, Penna A, Magenes G. A framework for the seismic assessment of existing masonry buildings accounting for different sources of uncertainty. Earthq Eng & Struct Dyn 2014;43(7):1045–66. https://doi.org/10.1002/eqe.2386.

[5] Ruggieri S, Liguori FS, Leggieri V, Bilotta A, Madeo A, Casolo S, et al. An archetype-based automated procedure to derive global-local seismic fragility of masonry building aggregates: META-FORMA-XL. Int J Disaster risk Reduct 2023;95:103903. https://doi.org/10.1016/j.ijdrr.2023.103903.

[6] Vargas L, Sandoval C, Bertolesi E, Calderón S. Seismic behavior of partially grouted masonry shear walls containing openings: experimental testing. Eng Struct 2023;278:115549. https://doi.org/10.1016/j.engstruct.2022.115549.

[7] Schuller MP. Nondestructive testing and damage assessment of masonry structures. Progress Struct Eng Mater 2003;5(4):239–51. https://doi.org/10.1002/pse.160.

[8] Ling L, Ma G, Hwang HJ, Tan X. Post-earthquake detection of surface spalling and cracks in masonry buildings based on computer vision (August). Structures, 78. Elsevier; 2025, 109226. https://doi.org/10.1016/j.istruc.2025.109226 (August).

[9] Milani G, Bertolesi E. Quasi-analytical homogenization approach for the non-linear analysis of in-plane loaded masonry panels. Construction and Building Materials, 146. Elsevier; 2017. p. 723–43. https://doi.org/10.1016/j.conbuildmat.2017.04.008.

[10] Rainone LS, Tateo V, Casolo S, Uva G. About the use of concrete damage plasticity for modeling masonry post-elastic behavior. Buildings 2023;13(8):1915. https://doi.org/10.3390/buildings13081915.

[11] Casolo S. Macroscale modelling of the orthotropic shear damage in the dynamics of masonry towers by RBSM. Eng Fail Anal 2021;130:105744. https://doi.org/10.1016/j.engfailanal.2021.105744.

[12] Kiureghian AD. A coherency model for spatially varying ground motions. Earthq Eng & Struct Dyn 1996;25(1):99–111. https://doi.org/10.1002/(SICI)1096-9845(199601)25:1<99::AID-EQE540>3.0.CO;2-C.

[13] Cantagallo C, Terrenzi M, Camata G, Spacone E. Historical evolution of the impact of seismic incident angles on the safety assessment of various building construction typologies. Buildings 2024;14(6):1490. https://doi.org/10.3390/buildings14061490.

[14] Mezzina M, Uva G. Edifici esistenti in muratura tra sicurezza e conservazione. Palazzo Carmelo a Cerignola 2022. CittàStudi. ISBN-10 8825174535. ISBN-13 978-8825174533.

[15] Dassault Systemes Simulia Corporation (2011). Abaqus (Version 6.11) [Computer software]. https://www.3ds.com/products-services/simulia/products/abaqus/.

[16] Lee J, Fenves GL. Plastic-damage model for cyclic loading of concrete structures. J Eng Mech 1998;124(8):892–900.

[17] Lubliner J, Oliver J, Oller S, Onate E. A plastic-damage model for concrete. Int J Solids Struct 1989;25(3):299–326.

[18] Lupoi A, Franchin P, Pinto PE, Monti G. Seismic design of bridges accounting for spatial variability of ground motion. Earthq Eng & Struct Dyn 2005;34(4-5):327–48. https://doi.org/10.1002/eqe.444.

[19] Shen J, Ren X, Chen J. Effects of spatial variability of ground motions on collapse behaviour of buildings. Soil Dyn Earthq Eng 2021;144:106668. https://doi.org/10.1016/j.soildyn.2021.106668.

[20] Ministero delle Infrastrutture e dei Trasporti. Aggiornamento delle «Norme Tecniche per le Costruzioni», Decreto Ministeriale 17 gennaio 2018. Suppl Ordin alla "Gazz Uff" N 42 Del 20 febbraio 2018 - Ser Gen 2018.

[21] Ministero delle Infrastrutture e dei Trasporti. Istruzioni per l'applicazione dell'«Aggiornamento delle "Norme tecniche per le costruzioni"» di cui al Decreto Ministeriale 17 gennaio 2018. Suppl Ordin alla "Gazz Uff" N 35 Del 11 febbraio 2019 - Ser Gen 2019.

[22] Giannopoulos D, Vamvatsikos D. Ground motion records for seismic performance assessment: To rotate or not to rotate? Earthq Eng Struct Dyn 2018;47(12):2410–25. https://doi.org/10.1002/eqe.3090.

[23] Larijani AK, Tehrani P. Investigating the effect of earthquake incident angle on seismic response and fragility analysis of irregular RC buildings with nonparallel systems (October). Structures, 68. Elsevier; 2024, 107135. https://doi.org/10.1016/j.istruc.2024.107135 (October).

[24] Shargh GB, Barati R. Probabilistic assessment of ground motion rotation impact on seismic performance of structures. Eng Struct 2023;292:116383. https://doi.org/10.1016/j.engstruct.2023.116383.

[25] Skoulidou D, Romão X, Franchin P. How is collapse risk of RC buildings affected by the angle of seismic incidence? Earthq Eng & Struct Dyn 2019;48(14):1575–94. https://doi.org/10.1002/eqe.3214.

[26] Zhang K, Zuo Z, Gong M, Wang X, Zhao Y, Liu B. The influence of forward-directivity pulse-like ground motion orientation angles on structural collapse capacity. Soil Dyn Earthq Eng 2025;191:109280. https://doi.org/10.1016/j.soildyn.2025.109280.

[27] Cannizzaro F, Pantò B, Lepidi M, Caddemi S, Caliò I. Multi-directional seismic assessment of historical masonry buildings by means of macro-element modelling: application to a building damaged during the L'Aquila earthquake (Italy). Buildings 2017;7(4):106. https://doi.org/10.3390/buildings7040106.

[28] Kesavan P, Menon A. A nonlinear static procedure for seismic assessment of unreinforced masonry buildings with rigid-diaphragms considering the effect of seismic incidence angle. Int J Mason Res Innov 2023;8(1):46–77. https://doi.org/10.1504/IJMRI.2023.127480.

[29] Kalkbrenner P, Pelà L, Sandoval C. Multi directional pushover analysis of irregular masonry buildings without box behavior. Eng Struct 2019;201:109534. https://doi.org/10.1016/j.engstruct.2019.109534.

[30] Ruggieri S, Uva G. Accounting for the spatial variability of seismic motion in the pushover analysis of regular and irregular RC buildings in the new Italian building code. Buildings 2020;10(10):177. https://doi.org/10.3390/buildings10100177.

[31] Uva G, Porco F, Fiore A, Ruggieri S. Effects in Conventional Nonlinear Static Analysis: Evaluation of Control Node Position (February). Structures, 13. Elsevier; 2018. p. 178–92. https://doi.org/10.1016/j.istruc.2017.12.006 (February).

[32] Cavaleri L, Papia M, Macaluso G, Di Trapani F, Colajanni P. Definition of diagonal Poisson's ratio and elastic modulus for infill masonry walls. Mater Struct 2014;47(1):239–62. https://doi.org/10.1617/s11527-013-0058-9.

[33] Bhaskar JK, Bhunia D, Koutas L. In-plane behaviour of masonry infill walls with openings strengthened using textile reinforced mortar (May). Structures, 63. Elsevier; 2024, 106439. https://doi.org/10.1016/j.istruc.2024.106439 (May).

[34] Casolo S, Diana V, Uva G. Influence of soil deformability on the seismic response of a masonry tower. Bull Earthq Eng 2017;15(5):1991–2014. https://doi.org/10.1007/s10518-016-0061-y.

[35] Dorji S, Derakhshan H, Thambiratnam DP, Mohyeddin A. Lateral load response of semi-interlocking mortarless masonry-infilled frames (March). Structures, 61. Elsevier; 2024, 105998. https://doi.org/10.1016/j.istruc.2024.105998 (March).

[36] Ferhi H, Attari N, Amziane S, Saidani M. Performance of limestone masonry walls under diagonal compression using innovative hybrid fiber-reinforced polymer (FRP) reinforcement techniques (December). Structures, 82. Elsevier; 2025, 110743. https://doi.org/10.1016/j.istruc.2025.110743 (December).

[37] Genç AF, Nasery MM, Cosgun SI, Yalçınyavuz AÜ. Damage simulations of the historic masonry aqueduct at Sümela monastery under rockfall and post-disaster landscape management. Eng Fail Anal 2025:110267. https://doi.org/10.1016/j.engfailanal.2025.110267.

[38] Izol R, Bayrak OF, Ilki A, Lourenco PB, Avcil F, Altunisik AC. Seismic behavior of historic square cross-section masonry minarets: The minaret of the Harran Ulu Mosque in Şanliurfa (Türkiye) (December). Structures, 82. Elsevier; 2025, 110504. https://doi.org/10.1016/j.istruc.2025.110504 (December).

[39] Pagni P, Bartolini G, De Falco A, Landi F, Resta C. The Use of Concrete Damage Plasticity for Modeling Shear-Compression Tests on Stone Masonry Panels (April). International Conference Florence Heri-Tech: the Future of Heritage Science and Technologies. Cham: Springer Nature Switzerland; 2024. p. 27–38 (April).

[40] Ram I, Senderovich S, Brodsky A. Experimental and Numerical Study on the Impact of Geometrical and Mechanical Properties of Joints on the Out-of-plane Behaviour of Masonry Walls (May). Structures, 75. Elsevier; 2025, 108849. https://doi.org/10.1016/j.istruc.2025.108849 (May).

[41] Roudane B, Kaya A, Adanur S. Nonlinear seismic damage analysis of low-rise masonry buildings using different materials. Eng Fail Anal 2025:110287. https://doi.org/10.1016/j.engfailanal.2025.110287.

[42] Drucker DC, Prager W. Soil mechanics and plastic analysis or limit design. Q Appl Math 1952;10(2):157–65.

[43] Duvaut G, Lions JL. Les Inequations en Mecanique et en Physique. Paris: Dunod; 1972.

[44] Lourenço PB, Rots JG, Blaauwendraad J. Continuum model for masonry: parameter estimation and validation. J Struct Eng 1998;124(6):642–52. https://doi.org/10.1061/(ASCE)0733-9445(1998)124:6(642).

[45] Park R. Evaluation of ductility of structures and structural assemblages from laboratory testing. Bull NZ Soc Earthq Eng 1989;22(3):155–66. https://doi.org/10.5459/bnzsee.22.3.155-166.

[46] Felicetta C, Russo E, D'Amico M, Sgobba S, Lanzano G, Mascandola C, et al. Istituto Nazionale di Geofisica e Vulcanologia. Italian Accelerometric Archive v 4.0. Dipartimento della Protezione Civile Nazionale; 2023. https://doi.org/10.13127/itaca.4.0.

[47] Luzi L, Hailemikael S, Bindi D, Pacor F, Mele F, Sabetta F. ITACA (ITalian ACcelerometric Archive): a web portal for the dissemination of Italian strong-motion data. Seismol Res Lett 2008;79(5):716–22. https://doi.org/10.1785/gssrl.79.5.716.

[48] Pacor F, Paolucci R, Luzi L, Sabetta F, Spinelli A, Gorini A, et al. Overview of the Italian strong motion database ITACA 1.0. Bull Earthq Eng 2011;9(6):1723–39. https://doi.org/10.1007/s10518-011-9327-6.

[49] Casolo S, Uva G. Seismic vulnerability assessment of masonry towers: full non-linear dynamics vs pushover analyses. Proc COMPDYN 2011 3rd Int Conf Comput Methods Struct Dyn Earthq Eng 2011:1–18.

[50] Casolo, S. (1994). A non-linear model for the study of the effects of 2-D ground motions on tall stone masonry structures. CIVIL-COMP PRESS, 10-Saxe-Coburg Place, Edinburgh, EH3 5BR, UK.